Fixed-Field Alternating-Gradient Particle Accelerators*

K. R. SYMON,† D. W. KERST,‡ L. W. JONES,§ L. J. LASLETT,‖ AND K. M. TERWILLIGER§
Midwestern Universities Research Association

(Received June 6, 1956)

It is possible, by using alternating-gradient focusing, to design circular accelerators with magnetic guide fields which are constant in time, and which can accommodate stable orbits at all energies from injection to output energy. Such accelerators are in some respects simpler to construct and operate, and moreover, they show promise of greater output currents than conventional synchrotrons and synchrocyclotrons. Two important types of magnetic field patterns are described, the radial-sector and spiral-sector patterns, the former being easier to understand and simpler to construct, the latter resulting in a much smaller accelerator for a given energy. A theory of orbits in fixed-field alternating-gradient accelerators has been worked out in linear approximation, which yields approximate general relationships between machine parameters, as well as more accurate formulas which can be used for design purposes. There are promising applications of these principles to the design of fixed-field synchrotrons, betatrons, and high-energy cyclotrons.

INTRODUCTION

ALTERNATING-GRADIENT (AG) focusing[1] provides a high degree of stability for both radial and vertical modes of betatron oscillations in circular particle accelerators. This stability makes possible the construction of many kinds of circular accelerators with magnetic guide fields which are constant in time, called fixed-field alternating-gradient (hereafter FFAG) accelerators. These machines contain stable equilibrium orbits for all particles from the injection energy to the output energy. These orbits may all be in an annular ring, as in a synchrotron or betatron; the magnetic field must then change rapidly with radius to provide orbits for the different energy particles. If the guide field gradient is made independent of azimuth, one of the modes of betatron oscillation is clearly unstable. Application of alternating-gradient focusing, however, can keep both modes of betatron oscillation stable even with the rapid radial change of magnetic field. Circular particle accelerators can be classified into four groups according to the type of guide field they use: fixed-field constant-gradient (conventional cyclotrons, synchrocyclotrons, and microtrons), pulsed-field constant-gradient (weak-focusing synchrotrons and betatrons), pulsed-field alternating-gradient (AG synchrotrons), and fixed-field alternating-gradient (FFAG synchrotrons, betatrons, and cyclotrons).

Two types of FFAG design appear the most practical. The radial-sector type[2] achieves AG focusing by having the fields in the successive focusing and defocusing magnets vary in the same way with radius but with alternating signs (or in certain cases alternating magnitudes). Since the orbit in the reverse field magnet bends away from the center, the machine is considerably larger than a conventional AG machine[1] of the same energy having an equal-peak magnetic field. This serious disadvantage is largely overcome in the spiral-sector type[3] in which the magnetic field consists of a radially increasing azimuthally independent field on which is superimposed a radially increasing azimuthally periodic field. The ridges (maxima) and troughs (minima) of the periodic field spiral outward at a small angle to the orbit. The radial separation between ridges is small compared to the radial aperture. The particle, crossing the field ridges at a small angle, experiences alternating-gradient focusing. Since the fields need not be reversed anywhere, the circumference of this machine can be comparable to that of an equivalent conventional AG machine.

FFAG synchrotrons have a number of important advantages over conventional synchrotrons. A major one is beam intensity. Since the magnetic field is time-independent in an FFAG synchrotron, the beam pulse rate is determined only by the repetition rate of the radio-frequency modulation cycle. In a conventional synchrotron, the beam pulse rate is limited by the time to complete the pulsed magnetic field cycle. It is reasonable to assume that frequency-modulation repetition rates can be made considerably higher than field recycling rates. Another reason for high beam intensity is the large injection aperture possible in the FFAG designs (larger for the radial sector than for the spiral sector). Other advantages of the FFAG synchrotron are engineering and maintenance simplifications. The direct-current magnet power supply is simpler and cheaper to construct and to maintain than a pulsed supply. The magnets do not have to be laminated, there are no eddy current problems, and remanent field and saturation difficulties are less serious than in pulsed-field

* Supported by National Science Foundation.
† University of Wisconsin, Madison, Wisconsin.
‡ University of Illinois, Champaign, Illinois.
§ University of Michigan and Michigan Memorial Phoenix Project, Ann Arbor, Michigan.
‖ Iowa State College Institute for Atomic Research, Ames, Iowa.

[1] Courant, Livingston, and Snyder, Phys. Rev. 88, 1190 (1952).

[2] K. R. Symon, Phys. Rev. 98, 1152(A) (1955). This structure was also suggested independently earlier by T. Ohkawa, University of Tokyo, Tokyo, Japan at a Symposium on Nuclear Physics of the Physical Society of Japan in October, 1953 (private communication), and independently by H. Snyder at Brookhaven National Laboratory.

[3] Suggested by D. W. Kerst [Kerst, Terwilliger, Jones, and Symon, Phys. Rev. 98, 1153(A) (1955)].

accelerators. All field trimming is time independent. The necessity for accurate tracking of the rf accelerating voltage with a pulsed magnetic field is eliminated, with a resulting greater freedom and ease in design of the rf system. Injection should be possible at a lower energy than is contemplated for a conventional synchrotron, because of the fewer low-field problems and the easier frequency-modulation program and the possibility of large apertures at the injection radius; the complexity of the injection system will then be decreased. Disadvantages of the FFAG synchrotron are the large increase in circumference for the radial-sector type (at least a factor of three) and the increase in complexity of the magnetic fields, particularly for the spiral-sector machine.

Fixed-field betatrons have potentially a much higher intensity than conventional betatrons.[4] The beam can be injected for a considerable fraction of a cycle, if extra accelerating flux is available, rather than the few tenths of a microsecond presently possible. The only beam current limitation appears to be space charge at injection, and this may be decreased by such techniques as high-voltage injection. An FFAG betatron has no problems of tracking a pulsed guide field with the accelerating flux, and also has other engineering simplifications mentioned in the synchrotron case.

Application of the FFAG principle to a cyclotron allows the radial dependence of the magnetic field to be such as to keep the particle revolution rate constant, independent of energy even in the relativistic region. Present high-energy cyclotrons must be frequency-modulated to compensate for the relativistic increase of mass. A constant-frequency cyclotron should increase the beam output by two orders of magnitude. A radial-sector cyclotron, in which the field alternates between high and low values, was first suggested by Thomas.[5] The spiral-sector design seems even more advantageous for application to the cyclotron.

In Part I of this paper we discuss the radial- and spiral-sector types of FFAG accelerator in detail. In Part II the theory of particle trajectories in FFAG machines is developed. Part III contains a description of a 10-Bev radial-sector synchrotron, a 20-Bev spiral-sector synchrotron, and FFAG betatrons and cyclotrons.

I. TYPES OF FFAG DESIGN

1. Radial-Sector Type

Circular particle accelerators with radial sectors can be built with the high-energy orbits at the outer edge of the machine and the injection orbits at the inside edge, or vice versa. This discussion assumes that the highest energy orbits are at the outside edge. (We will refer specifically to FFAG synchrotrons, but most of our comments will apply also to betatrons and cyclotrons.) In radial-sector design the magnet structure consists of N-identical sectors, each composed of a focusing magnet and a defocusing magnet. The magnet which is focusing for radial oscillations is of course defocusing for vertical oscillations and vice versa. The azimuthal boundaries of the magnets are on radii from the machine center (hence the name). The magnetic field direction in one magnet of a sector is opposite to that of the other, while the radial dependence of the field is the same in both. The field in the median plane at any azimuth is

$$H\sim(r/r_0)^k, \tag{1.1}$$

where r is the distance from the machine center to the equilibrium orbit and k is a constant for the machine. Figure 1 shows this type of field pattern. This field shape requires that orbits for different energy particles be similar, i.e., photographic images of each other. Ideally, the field along a closed equilibrium orbit is constant through each magnet, and the path is composed of arcs of circles. This ideal orbit cannot be attained because of the impossibility of a sharp field boundary. However, if we assume the ideal situation, a particularly simple case occurs if the fields for a given energy orbit have the same magnitude in the positive- and negative-field magnets. Equilibrium orbits for this case are shown in Fig. 2.

It is evident that particles deviating from the equilibrium orbit experience AG focusing. The numbers of radial and vertical betatron oscillations around the machine, ν_x and ν_z, are determined by k and the magnet lengths. Both ν_x and ν_z are constant for all energies.

It is desirable to make the negative-field magnets as short as possible, to keep the radius of the machine small; the minimum length of the negative-field magnet is of course determined by the necessity for preserving stability of the vertical betatron oscillations. Some vertical focusing and radial defocusing occur because the orbits are scalloped and do not cross the magnet edges at right angles. In machines in which the number of sectors is large and the effects of orbit scalloping small, the negative-field magnet can be made no shorter than about $\frac{2}{3}$ of the positive-field magnet if we wish to preserve vertical stability. This means that, neglecting

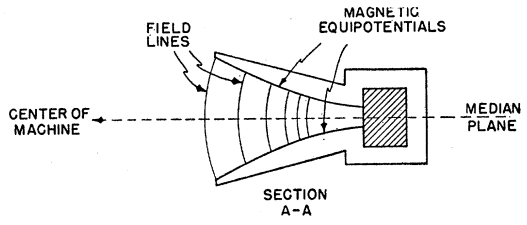

FIG. 1. Vertical section through positive or negative radial-sector magnets.

[4] Terwilliger, Jones, Kerst, and Symon, Phys. Rev. 98, 1153(A) (1955). This had been pointed out independently by G. Miyamoto, Tokyo University, Tokyo, Japan, at a meeting of the Physical Society of Japan in April, 1952 (private communication).

[5] L. H. Thomas, Phys. Rev. 54, 580, 588 (1938).

straight sections, the circumference of the machine is five times that which would be necessary if there were no negative-field magnets. The ratio (in this case, five) between the actual orbit circumference and the circumference of a circle whose radius is the minimum radius of curvature, we call the circumference factor. The fixed magnetic field in an FFAG machine can be made considerably larger than the pulsed field of a conventional accelerator, so a machine of the radial-sector type might actually be about three times the size of a pulsed-field AG accelerator of the same energy. It is also desirable to make the radial extent of the magnets as small as possible, which requires a high field gradient. The allowable gradient is determined by the effect of magnet misalignments. Reasonable values indicate a minimum radial aperture of about 2% of the radius of the machine.

2. Spiral-Sector Type

The spiral-sector design of FFAG accelerator has the high-energy orbits at the outside edge of the machine. It is not practical to have the high-energy orbits on the inside and to inject at the outside edge, because stability of the radial oscillations becomes virtually impossible to achieve.

The guide field on the median plane, if there are no straight sections, is given by

$$H=H_0(r/r_0)^k\{1+f\cos[N\theta-N\tan\zeta\ln(r/r_0)]\}, \quad (2.1)$$

where r is again the distance from the center of the machine; k, the mean field index; θ, the azimuthal angle, also measured from the center of the machine; f, the flutter factor (the fraction of field variation); N, the number of sectors (periods of the field variation) around the machine; and ζ is the spiral angle between the locus of the field maximum and the radius.

Figure 3 shows how the ridges and troughs of the periodic field spiral toward the outside of the machine and indicates the equilibrium orbits for this design. The equilibrium orbits are all similar figures, whose linear dimensions are proportional to the radius, but their positions rotate with radius due to the spiraling periodic field. Figure 4 is a plot of the radial dependence of the median-plane magnetic field. A particle going around the machine experiences a gradient first of one sign then of the opposite sign as it crosses the periodic field ridges and troughs at a small angle, so there is AG focusing of the betatron oscillations. The negative gradient is less than the positive gradient, due to the radial increase of field. This is somewhat compensated by the scalloping of the orbits, which causes the particle to experience a longer path in the negative gradient and a shorter path in the positive gradient than if it moved on a circle. The strength of betatron focusing depends on the rate of radial increase of the field, the flutter factor, and the spiral angle.

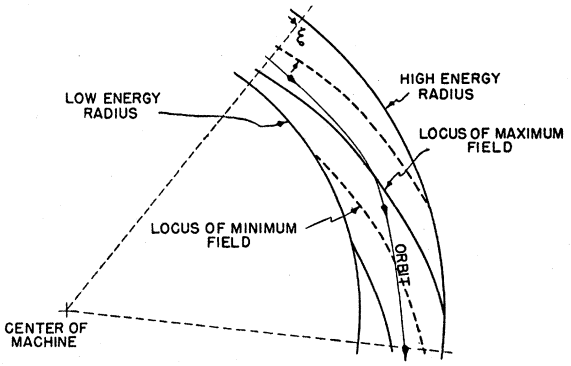

FIG. 3. Spiral-sector configuration.

The minimum size of radial aperture is limited primarily by the difficulty of achieving strong AG focusing with a periodic field while requiring a given vertical aperture. If we restrict ourselves to a sinusoidal variation of field, a flutter factor of $f=\frac{1}{4}$ gives the largest vertical gap for a fixed strength of focusing when iron magnet poles are used without distributed back windings and forward windings. This small flutter factor means that the machine has a circumference factor (in this case, $1+f$), close to unity, so the radius of an FFAG spiral-sector synchrotron is about the same as that of an equivalent-energy conventional synchrotron. The minimum radial aperture for reasonable parameters is about 3% of the radius.

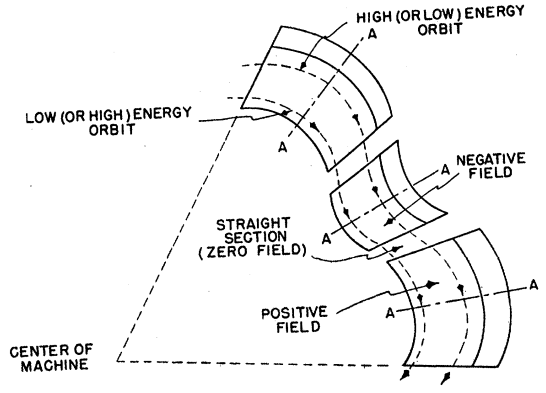

FIG. 2. Plan view of radial-sector magnets.

3. Other FFAG Types

Both the radial-sector and spiral-sector designs discussed above have equilibrium orbits of constant shape scaled in proportion to the orbit radius. There are many modifications of these designs. Some differ only in that the fields are not the square-wave type used in the radial-sector design described or the sinusoidal shape used in the spiral-sector design. Changes of this kind will not affect the constancy of shape of the equilibrium orbits and will modify other machine characteristics only slightly. There are other variations of these designs which preserve betatron oscillation

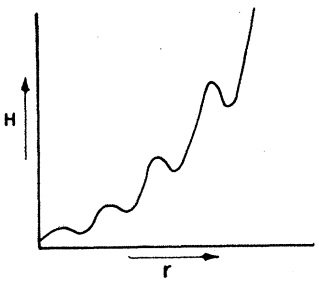

FIG. 4. Radial dependence of the axial magnetic field in the median plane.

stability, hold ν_x and ν_z constant, but do not retain the property of similarity of equilibrium orbits. The magnet edges of focusing and defocusing sectors can be made nonradial, and the fields in the positive- and negative-field magnets made different functions of radius; (the negative-field magnet can even be designed to have zero field). The magnet edges, radial or nonradial, can be tipped in the same direction, approaching the spiral-sector design. It is conceivable, using back windings, to transform from a spiral sector at the outside edge of the machine, with a small circumference factor where it is needed, to radial sector at the inside edge, with a large vertical aperture for injection. Such a design would have the advantages of both types with, however, a considerable increase in magnet complexity.

Another modification is the spiral-sector constant-frequency cyclotron. In this machine, the frequency of revolution of the particles can be made independent of energy even at relativistic energies, but the orbits in this case do not scale, and the number of betatron oscillations, ν_x and ν_z, cannot easily be kept constant.

II. ORBIT THEORY

4. Geometry of the Equilibrium Orbits

In order to develop a theory of orbit stability applicable to FFAG accelerators generally, it is convenient to characterize a particular accelerator by specifying its equilibrium orbits. We will therefore assume that a set of closed equilibrium orbits lying in the median plane is given. If instead, the magnetic field pattern is specified, the equilibrium orbits must be found by integrating the equations of motion.

The geometrical properties of each orbit, and the relations between orbits, will be periodic in the azimuthal angle θ with period $2\pi/N$. Each orbit is to be specified by its equivalent radius R defined by

$$S=2\pi R, \tag{4.1}$$

where S is the length of the orbit. In general, R will be slightly larger than the mean radius $\langle r\rangle_{Av}$. We define an azimuthal coordinate Θ by the equation

$$s=\Theta R, \tag{4.2}$$

where s is the distance measured along the orbit from some reference point (say at azimuthal angle θ_0). We shall require that the orbit be perpendicular to the radius from the center of the machine at the reference point, and that the reference points lie along a continuous curve. The parameter Θ will be equal to the azimuthal angle $\theta-\theta_0$ plus a small periodic function with period $2\pi/N$.

Each orbit will now be specified by a periodic parameter $\mu(\Theta,R)$ defined by

$$\mu(\Theta,R)=R/\rho(\Theta,R), \tag{4.3}$$

where ρ is the radius of curvature. Specification of $\mu(\Theta,R)$, together with the requirement that the center of the orbit lie at the origin in the median plane, completely determines the orbit R, provided the reference point $\Theta=0$ is specified. For our purposes, it will be sufficient to specify the angle $\zeta(R)$ between the radius from the origin and the reference curve $\Theta=0$ where it crosses the orbit R (Fig. 5). Choice of the parameter $\mu(\Theta,R)$ is restricted by the requirement that it be periodic in Θ with period $2\pi/N$ and mean value

$$\langle\mu\rangle_{Av}=\frac{1}{2\pi}\int_0^{2\pi}\mu d\Theta=\frac{1}{2\pi}\int_0^S\frac{ds}{\rho}=1. \tag{4.4}$$

The function $\mu(\Theta,R)$ is also restricted by the requirement that at the point $\Theta=0$ the orbit R must be perpendicular to the radius from the origin. This requirement leads to a rather complicated analytical restriction on the function μ. It is sufficient if $\Theta=0$ is a point of symmetry of the orbit, i.e.,

$$\mu(-\Theta,R)=\mu(\Theta,R). \tag{4.5}$$

If there are no points of symmetry, it is necessary to construct the orbit in order to locate properly the reference point $\Theta=0$. Fortunately, an error in properly locating the reference point will produce only a very small error (of order $1/N^2$) in the equations for the betatron oscillations, provided the angle ζ is correctly specified.

We will need also parameters $\eta(\Theta,R)$ and $\epsilon(\Theta,R)$ relating the perpendicular distance dx between two nearby orbits, and the increment $d\Theta$ in Θ along an orthogonal trajectory to the orbits, to the increment

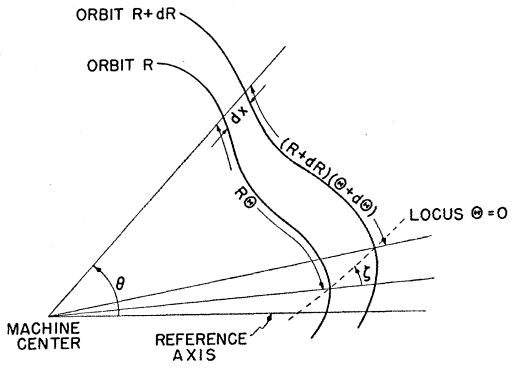

FIG. 5. Equilibrium orbit notation.

dR in the parameter R (see Fig. 5)

$$dx=\eta dR, \tag{4.6}$$

$$d\Theta=\epsilon dR/R. \tag{4.7}$$

It can be shown[6] that η, ϵ satisfy the differential equations

$$\frac{\partial\epsilon}{\partial\Theta}=\mu\eta-1, \tag{4.8}$$

$$\frac{\partial\eta}{\partial\Theta}=-\mu\epsilon-\int R\frac{\partial\mu}{\partial R}d\Theta, \tag{4.9}$$

where the three constants of integration are to be chosen so that ϵ and η are periodic functions of Θ [i.e., so that the right-hand members of Eqs. (4.8) and (4.9) have zero mean values], and so that

$$[\epsilon/\eta]_{\Theta=0}=\tan\zeta. \tag{4.10}$$

If all equilibrium orbits are geometrically similar, the parameter μ depends only on Θ and not on R. In the interest of simplicity, we will usually restrict our attention to machines of this type. If in addition, ζ is independent of R, then by Eqs. (4.8)–(4.10), the parameters η and ϵ will be independent of R. In this case, we will say that the equilibrium orbits *scale*; the equilibrium orbits scale if any set of neighboring orbits can be obtained by photographic enlargement or reduction from a set of orbits in the neighborhood of any other orbit.

The solution of Eqs. (4.8) and (4.9) may be obtained by successive approximations. Let us set

$$\mu=1+fg(N\Theta), \tag{4.11}$$

where $g(N\Theta)$ has period 2π in $N\Theta$, has mean value zero, and is normalized so that its mean square is $\frac{1}{2}$; f is the flutter factor. Since the right members of Eqs. (4.8) and (4.9) have period $2\pi/N$ (and zero mean), they contribute to η and ϵ oscillatory terms of order $1/N$. The integral in Eq. (4.9) is constant, if we assume that μ is independent of R; it will in any case contribute only very small oscillatory terms unless μ changes appreciably within a very small fractional increase in radius. The quantity $\tan\zeta$ is zero in radial-sector FFAG machines, but is of order N in spiral-sector FFAG machines. We therefore write as a zero-order approximation to η and ϵ the constant values

$$\eta\doteq 1, \quad \epsilon\doteq\tan\zeta, \tag{4.12}$$

which satisfy the conditions imposed on ϵ and η.

If $F(\xi)$ is any periodic function of ξ with period 2π, it is convenient to introduce the notations

$$\langle F\rangle_{Av}=\frac{1}{2\pi}\int_0^{2\pi}F(\xi)d\xi, \tag{4.13}$$

$$\{F\}=F(\xi)-\langle F\rangle_{Av}, \tag{4.14}$$

$$F'=dF/d\xi, \tag{4.15}$$

$$F_1=\int\{F\}d\xi, \tag{4.16}$$

$$F_{n+1}=\int F_n d\xi, \tag{4.17}$$

where the integration constants in the last two equations are to be chosen so that F_n has mean value zero. All the functions defined by Eqs. (4.14)–(4.17) have period 2π and mean value zero.

We now substitute Eqs. (4.11) and (4.12) in (4.8) and (4.9) and integrate again to get a first approximation

$$\eta\doteq 1-\frac{f\tan\zeta}{N}g_1(N\Theta), \tag{4.18}$$

$$\epsilon\doteq\tan\zeta-\frac{fg_1(0)}{N}\sec^2\zeta+\frac{f}{N}g_1(N\Theta), \tag{4.19}$$

where the integration constants have been chosen as required. [Note that

$$\langle g_1 g\rangle_{Av}=\frac{1}{2\pi}\int_0^{2\pi}g_1 dg_1=0, \tag{4.20}$$

and that if $g(\xi)$ is even, then $g_1(\xi)$ is odd, and $g_1(0)=0$. In any case, $g_1(0)$ is ordinarily small.]

A second approximation may be obtained by substituting η, ϵ from Eqs. (4.18) and (4.19) in the right members of Eqs. (4.8) and (4.9) and integrating again. Each successive iteration yields terms of order $1/N^2$ and f^2/N^2 times the preceding terms.

5. Betatron Oscillations

If a particle of momentum p moves in an equilibrium orbit R, then we have by Eq. (4.3)

$$pc=eH\rho=eHR/\mu, \tag{5.1}$$

where H is the magnitude of the magnetic field, so that

$$H(\Theta,R)=(pc/eR)\mu(\Theta,R). \tag{5.2}$$

The magnetic field is thus given in terms of the coordinates R and Θ.

If we differentiate Eq. (5.1) with respect to x, where x is measured perpendicular to the orbit, we have

$$H\frac{\partial\rho}{\partial x}+\rho\frac{\partial H}{\partial x}=-\frac{c}{e}\frac{\partial p}{\partial x}. \tag{5.3}$$

[6] K. R. Symon, Midwestern Universities Research Association report, MURA-KRS-8 (unpublished). A more elegant derivation has been given by B. Hamermesh and E. A. Crosbie [Argonne Accelerator Group, Progress Report No. 7, July 13, 1955 (unpublished)].

The field index is therefore

$$n=-\left(\frac{\rho}{H}\right)\frac{\partial H}{\partial x}. \qquad (5.4)$$
$$=\frac{\partial \rho}{\partial x}-\rho\frac{\partial \ln p}{\partial x}.$$

Making use of Eqs. (4.3), (4.6), and (4.7), we find

$$n=-\frac{1}{\eta\mu^2}\left[k\mu+\epsilon\frac{\partial\mu}{\partial\Theta}+R\frac{\partial\mu}{\partial R}\right], \qquad (5.5)$$

where k is a parameter which measures the momentum compaction:

$$k=R\frac{d\ln p}{dR}-1. \qquad (5.6)$$

In terms of the mean magnetic field $\bar{H}=pc/eR$, we can write k also as a mean field index:

$$k=\left(\frac{R}{\bar{H}}\right)\frac{d\bar{H}}{dR}. \qquad (5.7)$$

The linearized equations for betatron oscillations about an equilibrium orbit are[7]

$$\frac{d^2x}{ds^2}+\frac{1-n}{\rho^2}x=0, \qquad (5.8)$$

$$\frac{d^2z}{ds^2}+\frac{n}{\rho^2}z=0, \qquad (5.9)$$

where x and z are the deviations from the equilibrium orbit in the radial and vertical directions. These become, by Eqs. (4.2) and (4.3),

$$\frac{d^2x}{d\Theta^2}+\mu^2(1-n)x=0, \qquad (5.10)$$

$$\frac{d^2z}{d\Theta^2}+\mu^2nz=0. \qquad (5.11)$$

The character of the betatron oscillations is therefore determined by the functions $\mu^2(\Theta,R)$ and

$$\mu^2n=-\frac{1}{\eta}\left(k\mu+\epsilon\frac{\partial\mu}{\partial\Theta}+R\frac{\partial\mu}{\partial R}\right). \qquad (5.12)$$

By making use of Eqs. (4.8) and (4.9) we can rewrite Eq. (5.12) in the form

$$\mu^2(1-n)=\frac{(k+1)\mu}{\eta}-\frac{1}{\eta}\frac{\partial^2\eta}{\partial\Theta^2}. \qquad (5.13)$$

[7] N. M. Blachman and E. D. Courant, Rev. Sci. Instr. **20**, 596 (1949), Eq. (15).

If the equilibrium orbits scale, then μ, η, and ϵ are functions only of Θ. Thus μ^2n will be a function of Θ only, and the betatron oscillations will also scale provided k is constant. Accelerators with this property will be referred to as accelerators which scale. For accelerators which scale, we have

$$p=p_0(R/R_0)^{k+1}, \qquad (5.14)$$

and

$$H=H_0(R/R_0)^k\mu(\Theta). \qquad (5.15)$$

6. Approximate Solution for Betatron Oscillations

In this section we develop some approximate formulas which give a useful general picture of the properties of FFAG accelerators. If the betatron wavelengths are long in comparison with the sector length (say at least four sectors), then the smooth approximation equations developed in the appendix are applicable. The "smooth" betatron oscillation equations become in this case

$$d^2X/d\Theta^2+\nu_x^2X=0, \qquad (6.1)$$

$$d^2Z/d\Theta^2+\nu_z^2Z=0, \qquad (6.2)$$

where, by Eqs. (5.10), (5.11), and (A.13) of the appendix,

$$\nu_x^2=\langle\mu^2(1-n)\rangle_{Av}+\langle\{\mu^2(1-n)\}_1^2\rangle_{Av}, \qquad (6.3)$$

$$\nu_z=\langle\mu^2n\rangle_{Av}+\langle\{\mu^2n\}_1^2\rangle_{Av}. \qquad (6.4)$$

The solutions of Eqs. (6.1) and (6.2) are

$$X=A\cos\nu_x\Theta+B\sin\nu_x\Theta, \qquad (6.5)$$

$$Z=C\cos\nu_z\Theta+D\sin\nu_z\Theta. \qquad (6.6)$$

To these smooth solutions must be added a ripple which can be computed from Eq. (A.7). It is clear that ν_x and ν_z are the numbers of radial and vertical betatron wavelengths around the circumference of the accelerator. The approximate formulas (6.3) and (6.4) give ν_x and ν_z within about 10% provided that ν_x and ν_z are *both* less than $N/4$.

In order to avoid resonance buildup of betatron oscillations, it is necessary to avoid integral and half-integral values for ν_x and ν_z, and also to avoid integral values for $\nu_x+\nu_z$.[8] This implies that ν_x and ν_z must be the same for all orbits, or nearly so, and this is the principal limiting condition on FFAG designs. In accelerators which scale, ν_x and ν_z are necessarily the same for all orbits; this is the advantage in designs which scale.

The relation between betatron wavelengths and machine parameters depends upon which term in Eq. (5.13) predominates in giving alternating-gradient focusing. In a radial-sector FFAG accelerator with $\zeta=0$ and with a large number of sectors (say $N>10$),

[8] P. A. Sturrock, *Static and Dynamic Electron Optics* (Cambridge University Press, Cambridge, 1955), Chap. 7.

η is very nearly unity, and the second term in Eq. (5.13) is small except near the edges of the magnets where it gives rise to edge focusing effects. The edge focusing comes from the term $-(\epsilon/\eta)(\partial\mu/\partial\Theta)$ in Eq. (5.12). This term has a nonzero mean value, part of which is included in the μ term in Eq. (5.13); thus Eqs. (6.7) and (6.8) below include most of the mean focusing effect due to edges in radial sector machines. We will call the first term in Eq. (5.13) the "μ term" and the second, the "η term." In a spiral-sector FFAG accelerator, the alternating-gradient focusing comes predominantly from the η term. It may be noted that the η term includes the term $(R/\eta)(\partial\mu/\partial R)$ which appears when the orbits do not scale. It is not hard to see that in a conventional AG synchrotron[1] this is the dominant alternating-gradient term.

Let us first consider a radial-sector FFAG accelerator with a large number of sectors, and let us neglect the η term. If $f/N\ll 1$, then $\eta=1$ according to the discussion in Sec. 4. Let us write μ in the form given by Eq. (4.11). Then Eqs. (6.3) and (6.4) yield, if we substitute from Eq. (5.13), with $\eta=1$,

$$\nu_x^2=k+1+\frac{(k+1)^2f^2}{N^2}\langle g_1^2\rangle_{\text{Av}}, \tag{6.7}$$

$$\nu_z^2=-k+\frac{f^2}{2}+\frac{(k-1)^2f^2}{N^2}\langle g_1^2\rangle_{\text{Av}}, \tag{6.8}$$

where we have neglected a small term involving $\{g^2\}$ in Eq. (6.8). The betatron oscillation advances in phase by an angle

$$\sigma=2\pi\nu/N, \tag{6.9}$$

per sector. For stability,[1] σ should be less than π, and for the smooth approximation to be valid, σ must be less than about $\pi/2$. If we solve Eqs. (6.7) and (6.8) for k and f in terms of σ_x and σ_z, we obtain

$$k+1=\frac{N^2}{8\pi^2}(\sigma_x^2-\sigma_z^2+b), \tag{6.10}$$

$$f=\frac{4\pi}{[2\langle g_1^2\rangle_{\text{Av}}]^{\frac{1}{2}}}\frac{[\sigma_x^2+\sigma_z^2-b]^{\frac{1}{2}}}{|\sigma_x^2-\sigma_z^2+b|}, \tag{6.11}$$

where

$$b=\frac{4\pi^2}{N^2}\left[1+\frac{f^2}{2}-\frac{4kf^2}{N^2}\langle g_1^2\rangle_{\text{Av}}\right]. \tag{6.12}$$

The quantity b is negligible for sufficiently large N.

By appropriate choice of σ_x and σ_z, k can be made either positive or negative; i.e., in a radial-sector FFAG synchrotron, with N large, the high-energy orbits may be either on the outside or the inside of the donut. The b-term, which is important when N is small, is positive and therefore favors machines with positive k, i.e., with a given N, $|k|$ can be larger and f smaller if $k>0$. For maximum momentum compaction, i.e., minimum radial aperture, k, and hence N, should be as large as practicable. If we define a circumference factor C as the ratio between mean and minimum radii of curvature of the equilibrium orbit, then

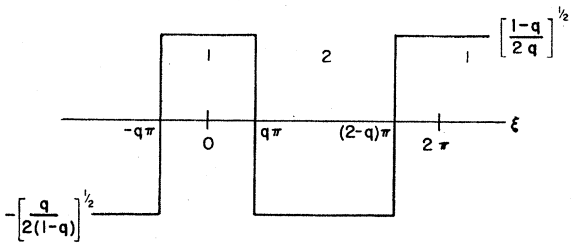

FIG. 6. Rectangular field flutter.

$$C=|\mu|_{\max}=|1+fg(N\Theta)|_{\max}. \tag{6.13}$$

It is desirable to minimize C, since for a given maximum magnetic field, this yields the smallest accelerator design. It is clear from Eq. (6.11), that for a given form of g, the minimum circumference factor is obtained by making σ_z as small, and σ_x as large as possible (or vice versa, if k is to be negative).

Let us assume a rectangular field flutter, with mean square value $\frac{1}{2}$:

$$g(\xi)=\left[\frac{1-q}{2q}\right]^{\frac{1}{2}}, \quad -q\pi<\xi<q\pi, \quad \text{(I)}$$
$$=-\left[\frac{q}{2(1-q)}\right]^{\frac{1}{2}}, \tag{6.14}$$
$$q\pi<\xi<2\pi-q\pi, \quad \text{(II)}$$

$$g(\xi+2\pi)=g(\xi). \tag{6.15}$$

This function is plotted in Fig. 6. When $\xi=N\Theta$ lies in regions labeled I, we say that Θ is in a positive half-sector; regions labeled II we call negative half-sectors. We need to calculate

$$\langle g_1^2\rangle_{\text{Av}}=\tfrac{1}{6}\pi^2q(1-q). \tag{6.16}$$

If now

$$K=f[\langle g_1^2\rangle_{\text{Av}}]^{\frac{1}{2}}, \tag{6.17}$$

is fixed by Eq. (6.11), then by Eq. (6.13), the circumference factor is

$$C=1+\frac{\sqrt{3}K}{\pi q}, \quad \text{or} \quad \frac{\sqrt{3}K}{\pi(1-q)}-1, \tag{6.18}$$

whichever is greater. The minimum value of C occurs when q is chosen so that the two values of the right member of Eq. (6.18) are equal. We then have

$$\mu=1+fg(N\Theta)=C, \quad -q\pi<N\Theta<q\pi, \quad \text{(I)}$$
$$=-C, \quad q\pi<N\Theta<2\pi-q\pi. \quad \text{(II)} \tag{6.19}$$

The radius of curvature, and consequently also the

magnetic field, is constant in magnitude along the equilibrium orbit and opposite in sign in the two half-sectors. The ratio of half-sector lengths is

$$\Gamma=q/(1-q)=(C+1)/(C-1), \tag{6.20}$$

and the circumference factor is

$$C=(\Gamma+1)/(\Gamma-1)=[1+\tfrac{1}{2}f^2]^{\frac{1}{2}}. \tag{6.21}$$

If we take $\sigma_z=\pi/6$, $\sigma_x=\pi/2$, $b=0$, and use the approximate formulas (6.10) and (6.11), we obtain $K=\sqrt{5}$, $\Gamma=1.31$, $C=7.5$, $f=10.5$, and $k=N^2/36$. It will be shown in the next section by a more accurate calculation that the minimum value of C where N is large is about 5.

In a spiral-sector FFAG accelerator, ζ is nearly 90° and the η term in Eq. (5.13) is large. It is then possible to use a much smaller flutter factor, so that the oscillatory part of the μ term is small. We will again assume that μ is given by Eq. (4.11) and will use the approximation (4.18) for η. If we expand $1/\eta$ in a power series in the second term of formula (4.18), we may calculate

$$\left\langle\frac{\mu}{\eta}\right\rangle_{\text{Av}}=1+\frac{f^2\tan^2\zeta}{N^2}\langle g_1^2\rangle_{\text{Av}}+\cdots. \tag{6.22}$$

We will neglect the second and higher order terms, and will neglect also the oscillatory part of μ/η. The η term can be rewritten in the following way:

$$\frac{1}{\eta}\frac{\partial^2\eta}{\partial\Theta^2}=\frac{\partial}{\partial\Theta}\left(\frac{1}{\eta}\frac{\partial\eta}{\partial\Theta}\right)+\left(\frac{1}{\eta}\frac{\partial\eta}{\partial\Theta}\right)^2. \tag{6.23}$$

The first term on the right is large and oscillatory with zero mean value, and the second is smaller but has a positive mean value. We neglect the oscillatory part of the second term, and substitute in Eqs. (6.3) and (6.4), using (5.13) to obtain

$$\nu_x^2=k+1, \tag{6.24}$$

$$\nu_z^2=-k+\tfrac{1}{2}f^2+2\left\langle\left(\frac{1}{\eta}\frac{\partial\eta}{\partial\Theta}\right)^2\right\rangle_{\text{Av}}. \tag{6.25}$$

Note that the η term does not contribute in this approximation to the radial focusing. If we take η as given by formula (4.18), we have

$$\left\langle\left(\frac{1}{\eta}\frac{\partial\eta}{\partial\Theta}\right)^2\right\rangle_{\text{Av}}$$

$$=f^2\tan^2\zeta\left\langle\frac{g^2}{(1-fN^{-1}\tan\zeta g_1)^2}\right\rangle_{\text{Av}}$$

$$=f^2\tan^2\zeta\left[1+\frac{2f^2\tan^2\zeta}{N^2}\langle g^2g_1^2\rangle_{\text{Av}}+\cdots\right]. \tag{6.26}$$

We will neglect the second and higher order terms in square brackets and substitute in Eqs. (6.24) and (6.25), to obtain

$$f^2\tan^2\zeta=(\nu_x^2+\nu_z^2-1), \tag{6.27}$$

where we have also neglected f^2. Note that, to this order of approximation, formulas (6.24) and (6.27) are independent of the form of the flutter function $g(N\Theta)$; only the circumference factor Eq. (6.13) depends on $g(N\Theta)$. We can rewrite these formulas in terms of the phase shifts σ per sector:

$$k+1=\frac{N^2\sigma_x^2}{4\pi^2}, \tag{6.28}$$

$$f^2\tan^2\zeta=\frac{N^2}{4\pi^2}(\sigma_x^2+\sigma_z^2)-1. \tag{6.29}$$

The reference curve $\Theta=0$, satisfies, in polar coordinates r and θ, the equation

$$\frac{1}{r}\frac{dr}{d\theta}=\cot\zeta. \tag{6.30}$$

The radial separation between ridges (points of maximum magnetic field), in units of r is therefore

$$\lambda=\Delta r/r=2\pi/(N\tan\zeta). \tag{6.31}$$

Thus for a given choice of σ_x, σ_z, and N the ratio f/λ is fixed. The maximum allowable gap between the poles of the magnet is proportional to λ; if the field flutter is to be obtained by shaping the poles, without extra forward windings, it can be shown (Sec. 13) that for f/λ fixed the maximum gap is about $\frac{1}{4}\lambda r$ and is obtained for $f\doteq\frac{1}{4}$. Under these conditions, the field flutter may be very nearly sinusoidal,

$$g(\xi)=\cos\xi, \tag{6.32}$$

and then the circumference factor will be $C=1+f=1.25$.

If we take, as above, $\sigma_z=\pi/6$, $\sigma_x=\pi/2$, with $f=\frac{1}{4}$, we obtain $k+1=N^2/16$, $\lambda=5.95N^{-2}[1-14.4N^{-2}]^{-\frac{1}{2}}$, and $\tan\zeta=1.05N[1-14.4N^{-2}]^{-\frac{1}{2}}$.

7. Linear Stability for Radial Sectors

In order to get more accurate relations between the parameters, we return to the betatron oscillation equations (5.10) and (5.11). Making use of Eqs. (5.12), (4.18), and (4.19), with $\zeta=0$, we rewrite Eqs. (5.10) and (5.11) for the case of a rectangular field flutter of the form (6.19):

$$\frac{d^2x}{d\Theta^2}\pm kCx=0, \tag{7.1}$$

$$\frac{d^2z}{d\Theta^2}\mp kCz=0, \tag{7.2}$$

where the upper signs apply in positive half-sectors, and the lower, in negative half-sectors. The term $\epsilon\partial\mu/\partial\Theta$ in Eq. (5.12) gives rise to terms in Eqs. (5.10) and (5.11) which represent the focusing that occurs at the sector edges, which we will neglect for the present. These approximations are valid only when $N\gg f$, and we have accordingly also neglected 1 in comparison with n. When N is small, edge effects and higher order terms in η must be taken into account. The oscillatory terms in η will give rise to effects resulting from the fact that neighboring equilibrium orbits are not everywhere equidistant. For small N, edge effects turn out to increase the vertical focusing and to decrease the radial focusing, so that considerably smaller values of the flutter factor f may be used if $k>0$, without losing vertical stability.

Let $N\Theta_0=-q\pi$, $N\Theta_1=q\pi$, $N\Theta_2=(2-q)\pi$. Then the solutions of Eq. (7.1) within the positive and negative half sectors separately yield the following matrix relations between x and $x'=dx/d\Theta$ at the points Θ_0, Θ_1, and Θ_2:

$$\begin{pmatrix} x_1 \\ x_1' \end{pmatrix}=M_+\begin{pmatrix} x_0 \\ x_0' \end{pmatrix}, \quad \begin{pmatrix} x_2 \\ x_2' \end{pmatrix}=M_-\begin{pmatrix} x_1 \\ x_1' \end{pmatrix}, \tag{7.3}$$

where

$$M_+=\begin{pmatrix} \cos\psi_+ & (kC)^{-\frac{1}{2}}\sin\psi_+ \\ -(kC)^{\frac{1}{2}}\sin\psi_+ & \cos\psi_+ \end{pmatrix},$$
$$M_-=\begin{pmatrix} \cosh\psi_- & (kC)^{-\frac{1}{2}}\sinh\psi_- \\ (kC)^{\frac{1}{2}}\sinh\psi_- & \cosh\psi_- \end{pmatrix}, \tag{7.4}$$

$$\psi_+=\frac{2\pi q}{N}(kC)^{\frac{1}{2}}, \quad \psi_-=\frac{2\pi(1-q)}{N}(kC)^{\frac{1}{2}}. \tag{7.5}$$

We thus obtain

$$\begin{pmatrix} x_2 \\ x_2' \end{pmatrix}=M\begin{pmatrix} x_0 \\ x_0' \end{pmatrix}, \tag{7.6}$$

with

$$M=M_-M_+=\begin{pmatrix} \cos\psi_+\cosh\psi_- -\sin\psi_+\sinh\psi_-, & (kC)^{-\frac{1}{2}}(\cos\psi_+\sinh\psi_- -\sin\psi_+\cosh\psi_-) \\ (kC)^{\frac{1}{2}}(\cos\psi_+\sinh\psi_- +\sin\psi_+\cosh\psi_-), & \cos\psi_+\cosh\psi_- +\sin\psi_+\sinh\psi_- \end{pmatrix}. \tag{7.7}$$

We can now calculate[8]

$$\cos\sigma_x=\tfrac{1}{2}\,\mathrm{trace}(M)=\cos\psi_+\cosh\psi_-, \tag{7.8}$$

and in the same way,

$$\cos\sigma_z=\cos\psi_-\cosh\psi_+. \tag{7.9}$$

In terms of the local field index

$$n=k/C, \tag{7.10}$$

within the magnets (we take n as positive here), and the ratio Γ of sector lengths [Eq. (6.20)], we may rewrite ψ_+ and ψ_-:

$$\psi_+=\left(\frac{2\pi}{N}\right)\left(\frac{\Gamma}{\Gamma-1}\right)n^{\frac{1}{2}}, \quad \psi_-=\left(\frac{2\pi}{N}\right)\left(\frac{1}{\Gamma-1}\right)n^{\frac{1}{2}}. \tag{7.11}$$

Formulas (7.5), (7.8), (7.9), and (7.11) have been written for $k>0$. However, they may also be used for $k<0$, in which case it is convenient to regard C as negative.

The smallest circumference factor is obtained by choosing σ_x as large as possible and σ_z as small as possible (or vice versa). If we choose $\sigma_x=3\pi/4$, $\sigma_z=\pi/6$. we calculate from Eqs. (7.8) and (7.9) that $\psi_+=1.32$, $\psi_-=1.93$. From Eqs. (7.11) and (6.21), we have

$$\Gamma=\psi_+/\psi_-=1.46, \quad C=5.35. \tag{7.12}$$

The theoretical minimum value of C is 4.45 for $\sigma_x=\pi$, $\sigma_z=0$. In order to keep the amplitude of betatron oscillations within reasonable bounds, the former choices of σ_x and σ_z run about as close to the stability limits as it is safe to go. (For the choice $\sigma_x=\pi/2$, $\sigma_z=\pi/6$, these more exact formulas give $\Gamma=1.29$, $C=7.9$, which may be compared with the approximate values 1.31, 7.5 obtained in the preceding section.)

A more general calculation, including straight sections between magnets, and taking edge effects into account, can be carried out in a similar way. We assume that along an equilibrium orbit the magnetic fields have equal and opposite constant values within the positive and negative half-sectors, and that the positive and negative half-sectors are separated by straight sections where the field is zero; (see Fig. 7). Let the fractions of orbit length within the positive and negative magnets be q_1 and q_2, respectively, and let the fraction of orbit

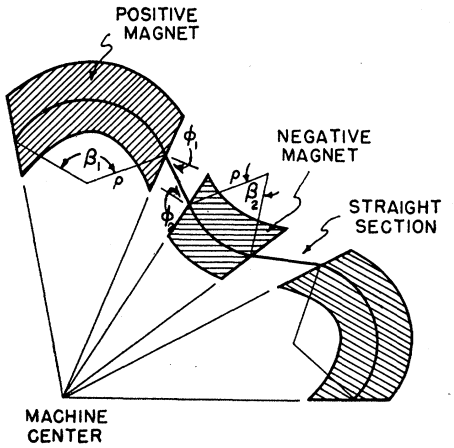

FIG. 7. Equilibrium orbit notation for radial sectors with straight sections.

length in each straight section be q_0, so that

$$2q_0+q_1+q_2=1. \tag{7.13}$$

The angles β_1 and β_2 shown in Fig. 7 are

$$\beta_1=2\pi Cq_1/N, \quad \beta_2=2\pi Cq_2/N. \tag{7.14}$$

The number of sectors is

$$N=2\pi/(\beta_1-\beta_2), \tag{7.15}$$

so that the circumference factor is

$$C=1/(q_1-q_2). \tag{7.16}$$

The angles ϕ_1 and ϕ_2 shown in Fig. 7 are the edge angles between the orbit and the normal to the magnet edges. It is convenient to define

$$\delta=2\pi Cq_0/N, \tag{7.17}$$

$$\psi_1=\beta_1(n_1+1)^{\frac{1}{2}}, \quad \psi_2=\beta_2(n_2-1)^{\frac{1}{2}}, \tag{7.18}$$

$$\psi_3=\beta_1 n_1^{\frac{1}{2}}, \quad \psi_4=\beta_2 n_2^{\frac{1}{2}}. \tag{7.19}$$

The indices n_1 and n_2 are the local field indices at the centers of the positive and negative magnets:

$$n=k/(\eta C), \tag{7.20}$$

where

$$\eta_1=1-2q_2\left(1-\frac{\sin(\pi Cq_2/N)}{Cq_2\sin(\pi/N)}\right)-2q_0\left(1-\frac{\cos(\pi Cq_2/N)}{(N/\pi)\sin(\pi/N)}\right), \tag{7.21}$$

and

$$\eta_2=1-2q_1\left(1-\frac{\sin(\pi Cq_1/N)}{Cq_1\sin(\pi/N)}\right)-2q_0\left(1-\frac{\cos(\pi Cq_1/N)}{(N/\pi)\sin(\pi/N)}\right). \tag{7.22}$$

We do not neglect 1 relative to n here. We do, however, neglect variation of η within the magnets. The result is

$$\begin{aligned}\cos\sigma_x=&[1+2\delta(\tan\phi_1+\tan\phi_2)+2\delta^2\tan\phi_1\tan\phi_2]\cos\psi_1\cosh\psi_2\\&+[(n_1+1)^{-\frac{1}{2}}(\tan\phi_1+\tan\phi_2+\delta\tan^2\phi_1+2\delta\tan\phi_1\tan\phi_2+\delta^2\tan^2\phi_1\tan\phi_2)-(n_1+1)^{\frac{1}{2}}(\delta+\delta^2\tan\phi_2)]\sin\psi_1\cosh\psi_2\\&+[(n_2-1)^{-\frac{1}{2}}(\tan\phi_1+\tan\phi_2+\delta\tan^2\phi_2+2\delta\tan\phi_1\tan\phi_2+\delta^2\tan^2\phi_2\tan\phi_1)+(n_2-1)^{\frac{1}{2}}(\delta+\delta^2\tan\phi_1)]\cos\psi_1\sinh\psi_2\\&+\tfrac{1}{2}[-(n_1+1)^{\frac{1}{2}}(n_2-1)^{\frac{1}{2}}\delta^2-(n_1+1)^{\frac{1}{2}}(n_2-1)^{-\frac{1}{2}}(1+\delta\tan\phi_2)^2+(n_1+1)^{-\frac{1}{2}}(n_2-1)^{\frac{1}{2}}(1+\delta\tan\phi_1)^2\\&+(n_1+1)^{-\frac{1}{2}}(n_2-1)^{-\frac{1}{2}}(\tan\phi_1+\tan\phi_2+\delta\tan\phi_1\tan\phi_2)^2]\sin\psi_1\sinh\psi_2,\end{aligned} \tag{7.23}$$

$$\begin{aligned}\cos\sigma_z=&[1-2\delta(\tan\phi_1+\tan\phi_2)+2\delta^2\tan\phi_1\tan\phi_2]\cos\psi_4\cosh\psi_3\\&+[n_2^{-\frac{1}{2}}(-\tan\phi_1-\tan\phi_2+\delta\tan^2\phi_2+2\delta\tan\phi_1\tan\phi_2-\delta^2\tan^2\phi_2\tan\phi_1)-n_2^{\frac{1}{2}}(\delta-\delta^2\tan\phi_1)]\sin\psi_4\cosh\psi_3\\&+[n_1^{-\frac{1}{2}}(-\tan\phi_1-\tan\phi_2+\delta\tan^2\phi_1+2\delta\tan\phi_1\tan\phi_2-\delta^2\tan^2\phi_1\tan\phi_2)+n_1^{\frac{1}{2}}(\delta-\delta^2\tan\phi_2)]\cos\psi_4\sinh\psi_3\\&+\tfrac{1}{2}[-n_2^{\frac{1}{2}}n_1^{\frac{1}{2}}\delta^2-n_2^{\frac{1}{2}}n_1^{-\frac{1}{2}}(1-\delta\tan\phi_1)^2+n_2^{-\frac{1}{2}}n_1^{\frac{1}{2}}(1-\delta\tan\phi_2)^2\\&+n_2^{-\frac{1}{2}}n_1^{-\frac{1}{2}}(-\tan\phi_1-\tan\phi_2+\delta\tan\phi_1\tan\phi_2)^2]\sin\psi_4\sinh\psi_3.\end{aligned} \tag{7.24}$$

8. Linear Stability for Spiral Sectors

For spiral-sector accelerators, the circumference factor is close to unity, and minimizing C is no longer a major consideration. The ridge separation λ is, however, rather small, and if the gap between magnet poles is to be kept as large as possible, it appears that the field flutter in the median plane must be at least approximately sinusoidal. We will therefore assume a field in the median plane of the form (2.1).

$$H=H_0(r/r_0)^k\{1+f\sin[N\theta-(1/w)\ln(r/r_0)]\}, \tag{8.1}$$

where we have set

$$1/w=N\tan\zeta=2\pi/\lambda. \tag{8.2}$$

The form of Eq. (8.1) is chosen so as to guarantee that the accelerator scales.

The linearized equations for the betatron oscillations in the field (8.1) can be obtained from the general analysis of the first two sections, but it is perhaps more illuminating to derive them directly. If one undertakes to write the linear terms in the differential equations characterizing the departure of the particle from a reference circle of radius

$$r_1=cp/[eH,(r_0/r_1)^k], \tag{8.3}$$

one obtains substantially the following:

$$r''+[1+k+(f/w)\cos N\theta](r-r_1)\doteq fr_1\sin N\theta, \tag{8.4}$$

$$z''-[k+(f/w)\cos N\theta]z\doteq 0. \tag{8.5}$$

These equations suggest alternating-gradient focusing of the type characterized by the Mathieu differential equation, but the presence of the forcing term on the right hand side of the equation for the radial motion indicates that a forced oscillation will be expected and will be given approximately by

$$r-r_1=-\frac{f}{N^2-(k+1)}r_1\sin N\theta. \tag{8.6}$$

Because of the presence of this forced motion, one realizes that not only will the nonlinear terms in the differential equations be large, but that a noticeable influence upon the betatron oscillation wavelength can result.

It is appropriate, therefore, to perform an expansion about a more suitable reference curve by writing

$$x=r-r_1+\frac{f}{N^2-(k+1)}r_1\sin N\theta. \quad (8.7)$$

In this way one obtains linearized equations, of which the most significant terms appear below:

$$x''+\left[k+1-\tfrac{1}{2}\frac{f^2/w^2}{N^2-(k+1)}+\frac{f}{w}\cos N\theta+\tfrac{1}{2}\frac{f^2/w^2}{N^2-(k+1)}\cos 2N\theta\right]x=0, \quad (8.8)$$

$$z''-\left[k-\tfrac{1}{2}\frac{f^2/w^2}{N^2-(k+1)}+\frac{f}{w}\cos N\theta+\tfrac{1}{2}\frac{f^2/w^2}{N^2-(k+1)}\cos 2N\theta\right]z=0. \quad (8.9)$$

These equations have the form of an extended Mathieu equation

$$d^2u/d\tau^2+(A+B\cos 2\tau+C\cos 4\tau)u=0. \quad (8.10)$$

The neglected terms in the coefficients A and C in Eq. (8.10) as given by Eqs. (8.8) and (8.9) are of order k^2w^2 times the main terms, so that for $f=\frac{1}{4}$, the error in these coefficients is less than 2% over most of the region of stability (Fig. 8). The neglected terms in the coefficients B are of order $\frac{1}{8}(f/N^2w)^2$ and $\frac{1}{2}(f/N^2w)^2$ in Eqs. (8.8) and (8.9), respectively, so that the errors will be less than 2% and 8%, respectively, over most of the region of stability. The coefficient of the third harmonic term (which has been omitted) is of order $\frac{1}{8}(f/N^2w)^2$ and $\frac{1}{2}(f/N^2w)^2$, respectively, times the coefficient B; since the third harmonic contributes to σ an amount proportional to $\frac{1}{9}$ the square of the coefficient, its contribution is completely negligible.

Tables of the characteristic exponent (σ/π) of the extended Mathieu equation (8.10) have been computed on the ILLIAC, using a variational method.[9] Values of A are tabulated for a range of values of σ, B, and C, covering the significant portion of the first stability region. Results for the Mathieu equation $C=0$ are included. So far as we are aware, there are at present no published tables of characteristic exponents for the Mathieu equation within the stability region.

In Fig. 8 we plot a stability diagram for a spiral-sector FFAG accelerator with $k\gg1$ computed from the above formulas and tabulated solutions of Eq. (8.20). If $k\gg1$, the coefficients A, B, and C depend only on k/N^2 and f/N^2w. We accordingly plot curves of constant σ_x and σ_z *vs* k/N^2 and f/N^2w. If we take $\sigma_z=\pi/6$ and $\sigma_x=\pi/2$, with $f=\frac{1}{4}$, we obtain $k=0.057N^2$, $f/N^2w=0.25$, and $\lambda=6.3N^{-2}$, which may be compared with the approximate values $k=0.062N^2$, $f/N^2w=0.265$, and $\lambda=5.95N^{-2}$ obtained at the end of Sec. 6.

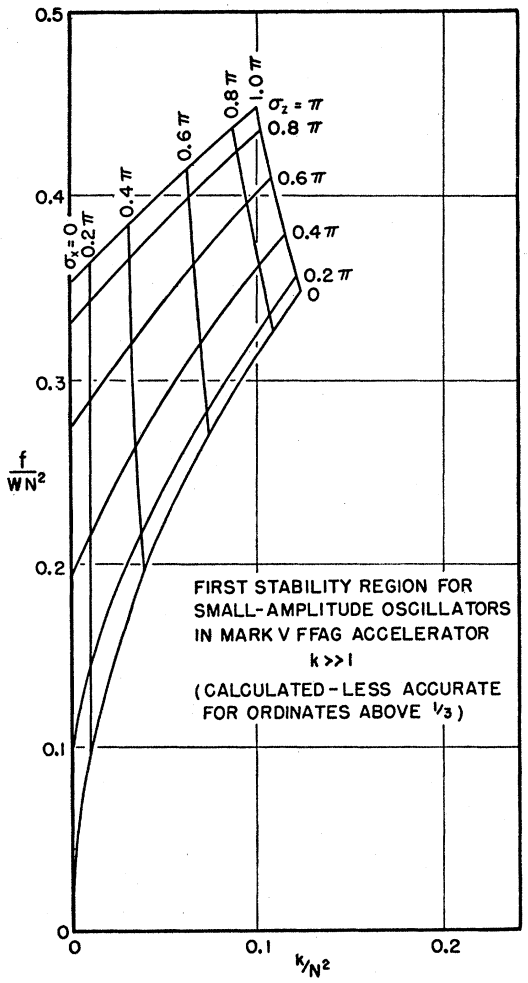

FIG. 8. Dependence of σ_x and σ_z within the stable region on spiral-sector parameters for $N\gg1$.

9. Nonlinear Effects

The preceding analysis of betatron oscillations has been based on an expansion of the equations of motion in powers of the displacement from the equilibrium orbit, keeping only the linear terms. The small-amplitude betatron oscillations in x and z are then found to satisfy linear differential equations with coefficients periodic in the independent variable Θ.

In a perfectly constructed accelerator, the only periodicity would be that associated with the N-identical sectors around the machine, and the period of the coefficients would be $2\pi/N$. In an actual accelerator, there will be imperfections, so that the coefficients will be

[9] Laslett, Snyder, and Hutchinson, "Tables for the determination of stability boundaries and characteristics exponents for a Hill's equation characterizing the Mark V FFAG synchrotron." Midwestern Universities Research Association Notes, April 20, 1955 (unpublished).

strictly periodic with the period 2π in Θ, and approximately periodic with period $2\pi/N$. Associated with the period $2\pi/N$ is the requirement that σ_x and σ_z must not be integral or half-integral multiples of 2π; in practice it appears that σ should be less than π, since otherwise the tolerances on magnet construction and alignment become very severe. Associated with the period 2π is the requirement that ν_x and ν_z must not be integral or half-integral if imperfection resonances are to be avoided, and, in addition, if imperfections can couple the x and z motions, $\nu_x+\nu_z$ must not be an integer.

The study of the effects of nonlinear terms in the equations of motion has not advanced nearly as far as the study of the linearized equations. Approximate analytic methods of treating nonlinear equations with periodic coefficients have been developed by Moser,[10] Sturrock,[8] and Hagedorn.[11] Their results can be summarized as follows: If the coefficients in the equations have period 2π in Θ, and ν_x, ν_z are the numbers of betatron oscillations in one period 2π, then resonances can occur when

$$n_x\nu_x+n_z\nu_z=\text{any integer, for}$$
$$n_x,n_z=0,1,2\cdots. \tag{9.1}$$

Let

$$n_x+n_z=q. \tag{9.2}$$

Then if $q=1$ or $q=2$, the motion is unstable even in linear approximation. (This is the rule stated in the preceding paragraph.) If $q=3$, then in general, the effects of quadratic terms in the differential equations are such as to make the motion unstable even at very small amplitudes. If $q=4$, then the effects of cubic terms may be to render the motion unstable, depending on the form of the cubic (and linear) terms. If $q>4$, then, in general, the motion is stable for sufficiently small amplitudes of betatron oscillation. In any case, if $q\geqslant 4$, and if the equations of motion are nonlinear, then there will be in general a limiting amplitude of betatron oscillations beyond which the oscillations are unstable at least in the sense that they leave the donut.

Numerical studies carried out on the ILLIAC at the University of Illinois seem to confirm these conclusions. It was also reported by the Brookhaven group[12] that experiments with the electron-analog alternating-gradient accelerator have confirmed these conclusions.

If we apply the above criteria to the sector periodicity $2\pi/N$, then we must replace ν_x and ν_z in Eq. (9.1) by $\sigma_x/2\pi$ and $\sigma_z/2\pi$, the number of betatron oscillations per sector. We then conclude for example that values of σ_x or σ_z near $2\pi/3$ are to be avoided, as well as values such that $\sigma_x+2\sigma_z$ or $\sigma_z+2\sigma_x$ is nearly 2π. We call these resonances with the periodicity of the structure itself "sector resonances." We have indeed found in numerical studies that the limiting amplitudes for betatron oscillations in spiral sector machines become very small when σ approaches $2\pi/3$.

If we apply the above criteria to the once-around period 2π, then we find that the values of ν_x and ν_z excluded by the above rules are as shown in Fig. 9. We plot ν_x horizontally and ν_z vertically. The lines labeled $q=1$, 2, 3, and 4 represent the values excluded by the above rules. The lines $q=1$ are integral resonances. The lines $q=2$ are half-integral resonances (vertical and horizontal) and sum resonances (diagonal). The lines $q=3$, 4 are third and fourth integral resonances. It is not yet altogether clear how serious the third and fourth integral resonances are, since they arise only from nonlinear imperfections in the machine. Experiments with the electron analog at Brookhaven[12] seem to indicate that these resonances must be excited by deliberately inserted nonlinear imperfections in order to be detected. This is not true of course of the $\sigma=2\pi/3$ resonances discussed in the preceding paragraph, which are resonances with the inherent periodicity of the structure. It would at present seem wise to avoid all the excluded lines on Fig. 9 if this can be done.

It should be pointed out that nonlinear terms in the equations for the radial sector accelerator are not very large, being not greater in order of magnitude than nonlinear terms which arise in some conventional alternating-gradient accelerators which have been contemplated. However, the nonlinear terms which arise when the sectors spiral are much larger and play a very important role in determining the character of

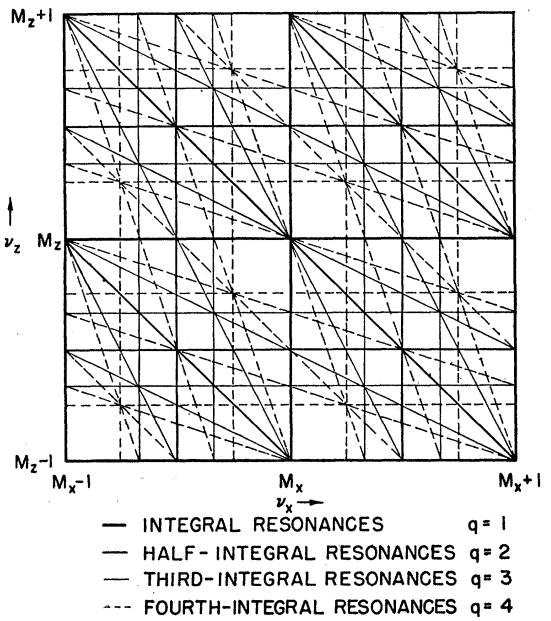

FIG. 9. Linear and nonlinear resonances in an AG accelerator. M_x and M_z are integers.

[10] J. Moser, Nachr. Akad. Wiss. Göttingen, Math.-physik. Kl. IIa, No. 6, 87 (1955). We are indebted to Dr. Moser for a very helpful discussion of his results.

[11] R. Hagedorn, CERN Report, CERN-PS/RH 9, November, 1955 (unpublished).

[12] Courant, Kassner, Raka, Smith, and Spiro, Phys. Rev. **100**, 1269(A) (1955).

the betatron oscillations. Numerical studies indicate that although the motion in spiral-sector synchrotrons exhibits marked nonlinear effects, the amplitude limits are large enough to accommodate reasonable betatron oscillations provided σ is not close to $2\pi/3$ (say $\sigma_x < 0.6\pi$).

10. Momentum Content and Phase Stability

The momentum $p(R)$ is determined by integrating Eq. (5.6):

$$p=p_0 \exp\left[\int_{R_0}^{R} \frac{k+1}{R} dR\right]. \tag{10.1}$$

If k is independent of R, this reduces to the simple relation (5.14). Thus momentum and energy are determined as functions of the orbit size R. Since R is essentially a mean radius of the orbit, the radial aperture required for any given initial and final momentum can be determined from Eq. (10.1). It is clear that for a given momentum content, the radial aperture decreases with increasing k. If $k \gg 1$, then the radial aperture is much less than R, and we have approximately, for constant k,

$$\frac{R_1-R_0}{R_0} \doteq \left(\frac{1}{k+1}\right) \ln\left(\frac{p_1-p_0}{p_0}\right). \tag{10.2}$$

The angular velocity of a particle in an orbit R is

$$\omega=\frac{d\Theta}{dt}=\frac{\beta c}{R}=\frac{pc^2}{ER}, \tag{10.3}$$

where E is the total energy, including rest energy. By squaring Eq. (10.3) and differentiating, we obtain

$$\frac{E}{\omega}\frac{d\omega}{dE}=\frac{1}{(E^2/E_0^2)-1}-\frac{1}{(R/E)(dE/dR)}. \tag{10.4}$$

We now differentiate the equation

$$E^2=p^2c^2+E_0^2, \tag{10.5}$$

and use Eq. (5.6) to obtain

$$\frac{E}{\omega}\frac{d\omega}{dE}=\frac{(k-1)E_0^2-E^2}{(E^2-E_0^2)(k+1)}. \tag{10.6}$$

We may integrate this equation if k is constant to obtain

$$\frac{\omega}{\omega_1}=\frac{E_1}{E}\left(\frac{E^2-E_0^2}{E_1^2-E_0^2}\right)^{k/[2(k-1)]}, \tag{10.7}$$

where ω_1 is the angular frequency of revolution at any particular energy E_1. A graph of ω/ω_t is shown in Fig. 10, where ω_t is the angular frequency at the transition energy, and we have taken $k=99$. If we define the transition energy

$$E_t=(k+1)^{\frac{1}{2}}E_0, \tag{10.8}$$

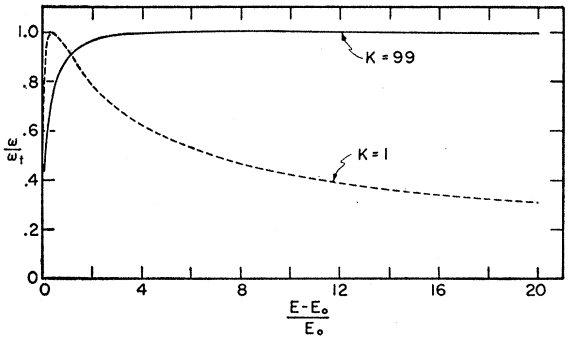

FIG. 10. Frequency of revolution as a function of energy.

then for $E<E_t$, $d\omega/dE$ is positive, while for $E>E_t$, $d\omega/dE$ is negative. If particles are accelerated by radio-frequency voltages applied to one or more accelerating gaps, then the theory of phase stability in FFAG accelerators is similar to that for conventional cyclotrons and synchrotrons.[13] When $d\omega/dE$ is positive, particles may execute stable synchrotron oscillations about a phase on the rising side of the voltage wave at the accelerating gap. When $d\omega/dE$ is negative, the stable phase is on the falling side of the voltage wave. At $E=E_t$, there is no phase stability. In order to accelerate particles beyond the transition energy, it is necessary to shift the relative phase at which the particle arrives at the accelerating gap from the rising to the falling side of the voltage wave.

In a cyclotron, the frequency of revolution, $\omega/2$, must be the same for all energies, and Eq. (10.6) then furnishes a relation between k and E:

$$k+1=E^2/E_0^2. \tag{10.9}$$

In a cyclotron, k must increase with energy, and the betatron oscillations therefore do not scale even when the equilibrium orbits scale.

III. APPLICATIONS

11. FFAG Proton Synchrotrons

As an illustration of the application of the FFAG principles to high-energy accelerator design, possible parameters are given below for a radial-sector and a spiral-sector synchrotron. Many of the considerations governing choices of parameters are common to these synchrotrons, and to pulsed-field alternating-gradient synchrotrons,[1] e.g., resonances, alignment tolerances, and gas scattering. It is anticipated that injection and acceleration might be accomplished somewhat differently than in pulsed-field synchrotrons of comparable energy.

Whereas injection from a 50-Mev proton linear accelerator is planned for 25-Bev pulsed-field accelerators, a 5-Mev Van de Graaf electrostatic generator might be

[13] D. Bohm and L. Foldy, Phys. Rev. **70**, 249 (1946); D. M. Dennison and T. H. Berlin, Phys. Rev. **69**, 542 (1946); R. Q. Twiss and N. H. Frank, Rev. Sci. Instr. **20**, 1 (1949).

used to inject into FFAG synchrotrons for the reasons mentioned in the introduction. Electrostatic-generator injection with FFAG synchrotrons would have the advantages of higher pulse currents, greater simplicity, lower cost, and better beam energy and size resolution than are at present realized with proton linear accelerators. Although one-turn injection using a pulsed inflector with a pulsed current of milliamperes is the most obvious injection system, many-turn injection may be used to give greater beam currents by scanning the aperture with the injected beam up to the space charge limit.

While the possibility of low-energy injection was evident when FFAG accelerators were conceived, it was also realized that it is usually uneconomical to use iron at a low flux density and that large momentum content in an FFAG accelerator requires much pole face area working at a very low flux density. This suggested the use of FFAG accelerators in succession with high flux density in the iron and with regenerative beam extractors used backward to inject particles from one accelerator into the next at high energy. Such regenerative peeler systems for extraction have been used for some time on betatrons and recently on cyclotrons; time reversal of the orbits would allow the system to be used for injection provided the injected beam can be caused to move away from the magnetic perturbation at the same time the excited oscillation in the beam is damped. This would require very careful adjustment. The feasibility of this sytem is being given extensive theoretical study by Teng,[14] and by others at the Argonne National Laboratory. Teng emphasizes that the use of high-energy injection largely avoids the frequency modulation problem and the problems of controlling the shape of low magnetic fields needed for low-energy injection. However, the radio-frequency modulation problem has many interesting possibilities of solution not available to pulsed-field accelerators.

The arbitrary frequency-*versus*-time program of FFAG synchrotrons allows the use of a mechanical modulation system with high-Q cavities. With the high Q realized in unloaded cavities, the required voltage gain per turn could be given the particles by one cavity driven at reasonable power. Modulation could be accomplished by moving a diaphragm to tune the cavity capacity. With such a system, model tests indicate a frequency change of a factor of 3:1 is practical. Using 5-Mev injection, a frequency change of 10:1 is required to reach relativistic velocities. One might then use one cavity operating as a self-excited oscillator to accelerate particles from injection to about 50 Mev. The voltage on that cavity would then be turned off as voltage on a second cavity is turned on, and acceleration continued with the second cavity. The change-over could be triggered by frequency comparison between cavities. The relative phases of the cavities could be controlled by a loose coupling between them. (With the University of Michigan electron synchrotron two-cavity rf system, it was observed that it was possible to make the transition from one cavity to another without an observable beam loss.) A third cavity might be added and a second transition made if desired, since it is observed that most of the energy is given the particles after they have reached almost constant velocity, c (see Fig. 10), and this third cavity could be designed to provide very high voltage over a small frequency range. Fine frequency adjustments would be made with reactance-tube loading of the cavities. With this rf system, it appears reasonable to accelerate protons to 20 Bev with a repetition rate of several per second.

While the above system is suggested on the basis of experimental tests already in progress, it is realized that other rf systems might prove more practical. Some of these are:

1. Many ferrite-loaded, low-voltage, low-Q cavities operated as tuned, driven amplifiers. Tuning would be accomplished by biasing the ferrites with currents. This is the system planned for the CERN and Brookhaven pulsed AG synchrotrons.

2. The use of drift tubes or operation of one or more entire magnet units as a drift tube on a high harmonic of the particle rotational frequency. In this case tuning over a wide frequency range appears difficult.

3. Several rf schemes have been proposed in which many groups of particles of different energies are present in the donut simultaneously. If any of these schemes proves practicable, large increases in duty factor and hence in beam output will become possible.

In alternating-gradient synchrotrons, phase stability vanishes at a transition energy, E_t, given by Eq. (10.8). It is possible in the radial-sector FFAG designs to have k large and negative. In this case there is no transition energy, and high-energy orbits lie on the inner radius of the machine. Negative-k designs appear to be not practical with spiral sectors. Figure 11 illustrates

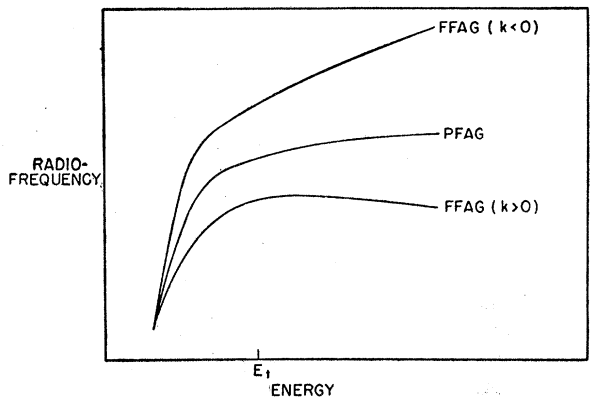

FIG. 11. Radio-frequency program for pulsed-field AG and FFAG synchrotrons.

[14] L. C. Teng, Phys. Rev. **100**, 1247 (1955).

qualitatively the radio-frequency *versus* energy program in a pulsed-field AG accelerator, and in comparable FFAG accelerators with positive and negative k.

12. A 10-Bev FFAG Proton Synchrotron with Radial Sectors

The following design for a high-energy proton synchrotron is intended to illustrate the features of the radial-sector FFAG synchrotron. This design type is at present the most completely understood of the FFAG accelerators thus far suggested, although spiral sectors certainly offer the possibility of more economical design. From the expressions (7.23 and (7.24), values of σ_x and σ_z may be found for a given choice of N, n, β_1, β_2, and δ. In Table I, typical values of the parameters are given for a 64-sector radial-sector accelerator. For this example we choose 10 Bev as the maximum proton energy and 20 000 gauss as the magnetic field for the equilibrium orbit of that energy. The limit on the strength of the focusing, radially and vertically, is set by the tolerances which must be placed on parameters of the machine such as n to avoid resonances. Since, if σ_x is kept constant, ν_x is roughly proportional to the square root of n, weaker focusing relaxes these tolerances. In cases where the simple expressions (7.8), (7.9) hold, the tolerance on n for $\Delta\nu=\frac{1}{2}$ is, by differentiating,

$$\frac{dn}{n}=\frac{2\pi\sin\sigma}{N(\psi_1\sin\psi_1\cosh\psi_2-\psi_2\cos\psi_1\sinh\psi_2)}. \quad (12.1)$$

For the above design figures, the tolerance on n is about one percent. A closer tolerance might be held on n in the fixed-field case than in the pulsed-field case since all field adjustments are time-independent.

Misalignment of magnets in alternating-gradient accelerators has been shown to give rise to large deviations of equilibrium orbits.[15] In radial-sector accelerators, the equilibrium orbit deviation for a given rms sector misalignment may be shown[15] to be worse, by approximately the ratio of circumference factors, than in a conventional AG accelerator of the same number of magnet units and comparable ν_x and ν_z. Here the simplifying assumptions are made that misalignments occur for magnet units as a whole, and that they are random and independent. For the accelerator in this example, an rms misalignment of the 128 magnets of 0.02 cm would be expected to result in a maximum deviation of the equilibrium orbit of ± 2.0 cm.

TABLE I. Illustrative values of the parameters for a radial sector accelerator.

$N=64$	$\beta_1=15.00°$	$\sigma_x=122.1°$
$n_1\doteq n_2=36$	$\beta_2=9.37°$	$\sigma_z=22.0°$
$C=5.35$	$\delta=0.05°$	$\nu_x=21.7$
$k=192.5$	$\phi_1\doteq\phi_2=5.74°$	$\nu_z=3.91$

TABLE II. Physical dimensions of a radial sector accelerator. Subscript 0 refers to maximum energy, subscript i refers to injection.

$E_0=10$ Bev	$E_i=5$ Mev	proton kinetic energy
$r_0=97.3$ m	$r_i=95.0$ m	synchrotron radius
$B_0=20\,000$ gauss	$B_i=200$ gauss	magnet guide field
$\rho_0=18.2$ m	$\rho_i=17.8$ m	radius of curvature
$Z_0=3.0$ cm	$Z_i=15.0$ cm	vertical semiaperture
$r_0-r_i=2.3$ m	radial aperture	
$E_t=12$ Bev	transition energy	
$Z_i=2.5$ cm	vertical semiheight of injected beam	
$\delta_i=\pm 0.001$ radian	angular spread of injected beam	
$p=5\times10^{-6}$ mm Hg	pressure in the vacuum chamber	

The effects of space charge and gas scattering have been treated by Blachman and Courant[16] and others.[17] In this example, an injected beam from a typical Van de Graaf electrostatic accelerator would fill ± 10 cm of aperture after gas scattering. Adiabatic damping of betatron oscillations as the momentum increases by a factor of 100 during acceleration would then reduce these oscillations to ± 1.0 cm. At a reasonable rate of acceleration (75 kilovolts per turn), 3×10^{11} protons per pulse could be accepted.

The values of physical quantities consistent with the parameters of Table I and the above considerations are given in Table II.

Figure 12 illustrates in cross section a possible method of constructing the magnets. Much of the large change in field would be accomplished by back-winding coils on the pole sufaces. Table III illustrates the magnet parameters for the accelerator described above in Tables I and II.

With the rf system described above, the repetition rate is limited only by the rf voltage which can be applied and by the rate of mechanical frequency modulation attainable. Using this rf system with the accelerator of this illustration, one to three pulses per second of 3×10^{11} ten-Bev protons appear attainable.

13. 20-Bev FFAG Proton Synchrotron with Spiral Sectors

As an example of an accelerator made with a ring magnet producing loci of maximum field which cross the path of the particle at a small angle, we take a field of the form (8.1). The motion for this case is treated in Part II. Equations (6.24), (6.27), and (6.31) show that in the smooth approximation

$$\nu_x^2=1+k, \quad (13.1)$$

$$\nu_z^2=-k+(f/wN)^2+\tfrac{1}{2}f^2, \quad (13.2)$$

[15] E. D. Courant and H. S. Snyder, Internal Brookhaven National Laboratory Report, June 1, 1953 (unpublished); G. Lüders, CERN reports CERN-PS/GL 4, GL6, GL7, GL8, and GL9 (unpublished); E. Crosbie, Argonne Accelerator Group, Progress Report No. 5, February 24, 1955 (unpublished).

[16] N. M. Blachman and E. D. Courant, Phys. Rev. **74**, 140 (1948); **75**, 315 (1949).

[17] J. Seiden, Compt. rend. **237**, 1075 (1953); D. W. Kerst, Phys. Rev. **60**, 47 (1941); J. P. Blewett, Phys. Rev. **69**, 87 (1946).

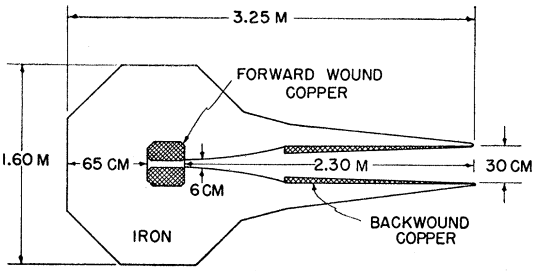

FIG. 12. Cross section of radial-sector magnet and coils.

where $w=\lambda/2\pi$ and λ is the radial separation between adjacent ridges in units of the radius.

Parameters for a 20-Bev ring magnet will be derived using this smooth-approximation result and the condition $\sigma=2\pi\nu/N<\pi$, the stability limit for a Hill equation. Later the alteration of these parameters resulting from exact solution of the linearized differential equation by the use of the Illiac digital computer will be shown.

We can choose from many types of injectors—linear accelerators of 50 Mev, cyclotrons, or, for much lower energy, Van de Graaf electrostatic accelerators. For the purpose of this example, suppose we choose an extreme case in which the ring magnet is able to hold orbits of 5-Mev injected protons at its inside rim and orbits of 20-Bev protons at its outside rim. We can choose $k=82.5$, $r_0=5000$ cm, where r_0 is the mean radius of the high-energy orbit using 14 000 gauss for the average field strength at the orbit. This gives $r_i=4688$ cm as the mean radius of the 5-Mev orbit. A radial extent of the magnet gap of approximately $d=r_0-r_i=312$ cm is needed. The ratio of the average field at the high-energy orbit to the average field at the low-energy orbit is $\bar{H}_0/\bar{H}_i=203$.

Since $k=82.5$, $\nu_x=9.15$ radial betatron oscillations around the machine according to the smooth approximation. To remain within the stability limit for the linearized differential equation with varying coefficients we must have $2\nu<N$. Choose $N=31$ sectors or ridges crossed in one passage around the machine. This gives $\sigma_x=0.6\pi$. We can then choose $\sigma_z=0.268\pi$, so that $\nu_z=4.15$. This choice of ν_x and ν_z avoids the forbidden lines on Fig. 9. The working point chosen is then in one of the two largest squares available in (ν_x,ν_z) space. The ridge characteristics can now be found by the second smooth approximation Eq. (13.2) which gives $f/w=218$ with the above values of N and k.

Thus if we take $f=\frac{1}{4}$, then $\lambda=0.00506$ in units of the radius, so that the radial separation of the ridges at the outside edge is 25.3 cm. This result is only approximate.

TABLE III. Magnet parameters characterizing a radial sector accelerator.

Total weight of iron	9650 tons
Total weight of copper	670 tons
Required current	112 000 ampere turns
Required magnet excitation power	5.5 megawatts

The accurate solution to the linearized equations can be summarized in the form shown in Fig. 8 which exhibits the "necktie" for the case of a magnetic field of our prescribed form in the median plane. According to this diagram, take $\sigma_x=0.615\pi$ and $\sigma_z=0.25\pi$; then $f/wN^2=0.303$ and $k/N^2=0.075$. If we choose $N=33$ sectors, we have: $\nu_x=10.15$, $\nu_z=4.15$. Both values are now in the middle of a different large square allowed by the integral, half-integral, and third integral rules. (To be in the center of the largest allowed squares, the working point ν_x, ν_z should be 0.15 units above integers for both dimensions or 0.15 units below integers for both dimensions.) If we again take $f=\frac{1}{4}$, then $w=1/1320$, so $\lambda r_0=23.8$ cm radial ridge separation.

At this point, consideration must be given to the possible magnitude of f which can be achieved. The shapes of magnetic potential surfaces which will produce a flutter $f=\frac{1}{4}$ with $k=150$ are shown in Fig. 13. The

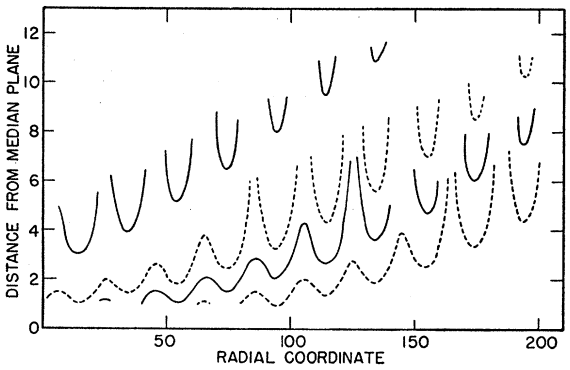

FIG. 13. Spiral-sector equipotentials for $k=150$ and $f=0.25$. Ordinates and abscissas are in the same units.

curves are loci of constant magnetic potential for several different values of the potential. These curves were determined by digital computation. They show deep crevices developing in the surfaces or poles when the ridge is about 0.13λ away from the median plane. Apparently when the gap between ridges exceeds $\frac{1}{4}$ of the radial separation of the ridges, the crevices in the surfaces occur. These crevices mean that a pole of opposite polarity is needed in the crevices to produce the required flutter when the gap is large. If we do not want pole faces with these reverse poles embedded in them, then the gap between ridges must not exceed one fourth of the radial separation of the ridges. The same result has been obtained analytically.

Figure 14 shows the calculated shape of the equipotential surfaces for $f=\frac{1}{4}$. The dependence of gap is shown in Fig. 15 where G is the maximum gap at ridge tops without forward windings. If we require that the ν's be constant, f/w must be constant. Thus we plot Gf/w *vs* f in Fig. 1. We see that the flutter f which gives the maximum possible gap at the ridges, under

conditions of constant alternating-gradient focusing, that is, constant f/w, is $f=\frac{1}{4}$, and the maximum gap is $G=0.275$ in units of the ridge separation. The curves show that flutter factors from 0.14 to 0.36, without crevices in the poles, require that the gap be only 10% less than the maximum possible gap. These analytical results are similar to those from digital computation as already mentioned.

For the example we are considering, we had $\lambda r_0 = 2\pi w r_0 = 23.8$ cm radial separation between ridges at r_0. This means that if we choose $G=0.275\lambda r_0$, then $G=6.15$ cm at the injection radius and 6.6 cm at the high-energy radius.

To make the magnetic field 203 times larger at the high-energy radius than at the injection radius, this gap would have to be reduced by a factor of 203 unless currents are distributed on the pole face. By placing such windings between iron ridges, the gap can be kept full size at all radii. Thus, by proper winding, $G(r)$ could always be about 0.275 times the ridge separation,

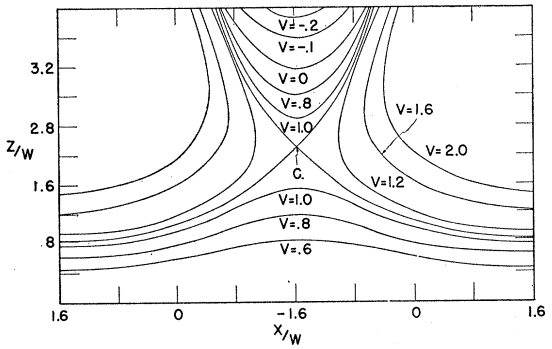

FIG. 14. Magnetic potentials, $V=Z/W+f\sin(X/W)\sin[H(Z/W)]$, for $k=0$ and $f=0.25$. Poles corresponding to $V=1.1$ have the widest gap without crevices in the pole surface.

which is practically constant. However, it is not most desirable to have the gap essentially constant at all radii because the amplitude of betatron oscillations decreases as $p^{-\frac{1}{2}}$ while the particle is being accelerated. Thus if the momentum increases by a factor of ~ 203, then the space required for betatron oscillations decreases by a factor of $(200)^{\frac{1}{2}}$ or ~ 14. Consequently it would be best to have the gap at the injection radius about 10 times larger than the gap at high energy and it would be desirable to fill this large aperture with beam at the injection time. Actually the gap at successive energies should be big enough to accommodate not only the decreasing betatron oscillations but also the misalignment distortion of the equilibrium orbit. If we maintain a gap as large as possible without the addition of opposite poles between ridges, that is if we keep $G=0.275\lambda r$, then the aperture available actually increases slightly during acceleration due to the slight increase in r. To reverse this gap variation without decreasing the gap below about 6.2 cm would require

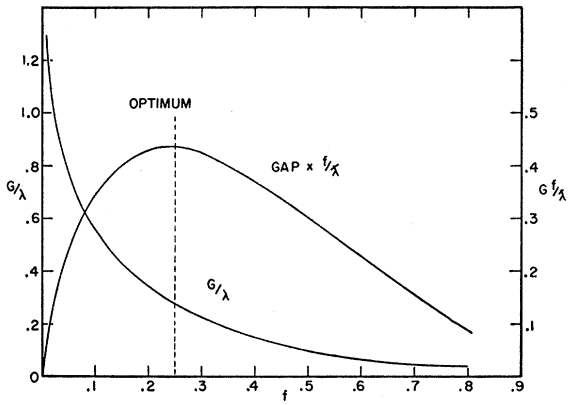

FIG. 15. Maximum gap, G, times (f/λ), for fixed tune as a function of f. The criterion of no crevice in the pole face is used. The field variation in the orbital plane is sinusoidal.

introduction of reverse poles between ridges where it is most easily done, that is at the low-field rim. In practice this can be accomplished by running currents in two directions between a few of the low-field ridges. Then the iron surfaces may be separated farther to give an increased vertical aperture. It seems reasonable that the gap at the injection radius could be doubled this way.

A configuration of the ridges and coils which produces the correct field shape is shown in Fig. 16 which shows iron contours as magnetic equipotentials. The location of current-carrying copper between the ridges is shown. This current terminates some magnetic potential surfaces, allowing the iron to be brought down to the same gap magnitude at successive ridges. Since the magnetic field decreases by the same factor between all adjacent ridges, the amount of back-wound current in the slot decreases by the same factor between slots. Thus the slot at the high-field ridge carries the largest number of back-wound ampere turns. The figure shows how the gap at the injection radius might be doubled by using forward and backward currents in the slot. Such a magnet requires about 1.8 megawatts of power.

With this method of providing the field shaping, it would be necessary to carry current over the ridges of iron as they spiral outwardly. A way to do this is to have the gap between ridge tops close a little as they spiral outward to produce the field increasing as r^k, and then to have the wires carrying current come back to the

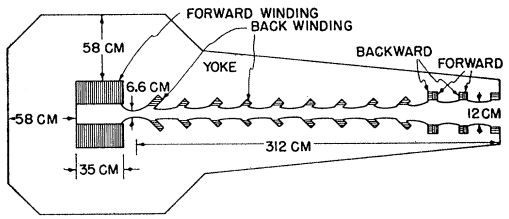

FIG. 16. Spiral-sector magnetic structure. The insertion of back-wound current carrying conductors allows the gap between the poles to be about the same for all ridges.

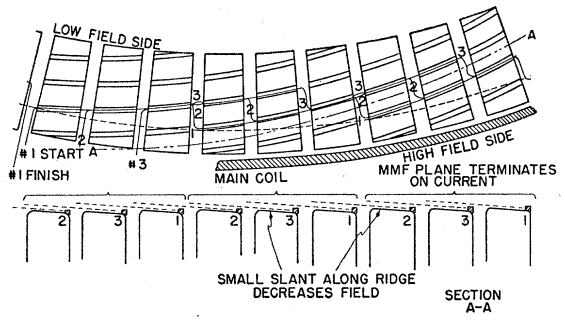

FIG. 17. Method of bringing conductors back across ridges at straight sections.

beginning radius at the start of the next sector around the magnet. Straight sections between sectors provide the opportunity to bring the conductors back to the same radius. Since the field changes by about 35% from ridge to ridge, the gap would have to change by about 35% between the crests of ridges from one end of a sector to the other. A less drastic change in gap along ridges results if the sectors, which are about 32 feet long, are subdivided say 3 times to form approximately 10-foot lengths with straight sections between. Then the gap needs to vary only about 12% along a ridge top and the wires between ridges can come back to the same radius every 11 feet around the circumference. This is shown in Fig. 17.

This brings up the problem of straight sections where the magnet is separated and where the field is approximately zero. If such cuts in the magnet are made along approximately radial lines, the machine and the orbits do not scale. Consequently σ varies periodically as the radius of the orbit grows. This problem is one of the most important being studied by the MURA technical group and there are indications that the distribution of the straight sections, such as subdivision of sectors into several parts as just mentioned, minimizes the variation of σ to a tolerable value with a useful length of straight section.

There is another example of a method to attain the desired field shape which simplifies some of the problems and which has been studied in the form of magnetic models by the MURA technical group. Such a structure is shown in Fig. 18. The average radial dependence of field (r^k) is produced by back-windings on iron poles similar to those used in a radial-sector magnet. The magnetic equipotential surfaces so formed are distorted or kinked by some other means such as the presence of iron rods having the same shape as the desired magnetic equipotentials on the side toward the orbits. These rods assume their magnetic potential from their positions in the gap. Since the rods spiral from one radius to another, they must be segmented with a few nonmagnetic spacers such as brass washers to prevent magnetic flux from traveling along the rod. Such ridges and the proper fields were achieved in the models made by F. L. Peterson and T. B. Elfe of the MURA technical group.

An interesting observation which they made shows that there is the possibility of relaxing the requirements for a small gap in a spiral sector magnet. They were able to increase f greatly above the design figure of $\frac{1}{4}$ without closing the gap and without using reverse poles or deep crevices between ridges. It was done merely by deviating slightly from a simple sinusoidal field variation. A value of $f\sim0.38$ was reached without a great harmonic distortion of the field in the median plane. Further studies of this possibility will be needed to show how much the alternating-gradient term in ν_z is increased by the attainable field shapes. Any increase would allow opening the gap more.

An important question must be answered before it is known how large a gap is useful. As pointed out in Sec. 9, the motion of a particle in a magnetic field which causes nonlinear restoring forces generally has a limit to the amplitude for stable motion or an amplitude limit beyond which the particle starts to oscillate about a second closed equilibrium orbit in or outside the accelerator. If oscillation about this second orbit takes the particle out of the aperture, the particle is lost. In the radial direction this limit can be as large as 0.1 to 0.3 of a ridge separation and in the axial direction it is smaller. The example given does not have an especially large limit because σ_x is near $2\pi/3$. The increase of such stability limits by suppression of some of the nonlinear forces would make it worthwhile to open the gap farther than 0.275 of the ridge separation because more vertical space useful for betatron oscillations would become available. For some vertical stability limits observed with the digital computer, there would be no value in opening the gap wider because the stability limit is within the gap available. The sources of the nonlinear effects are being studied with the purpose of designing a spiral-sector system to make larger gaps useful. In general, if the angle ζ is made smaller so the oscillations do not cause a large variation in sector length, the stability limit increases.

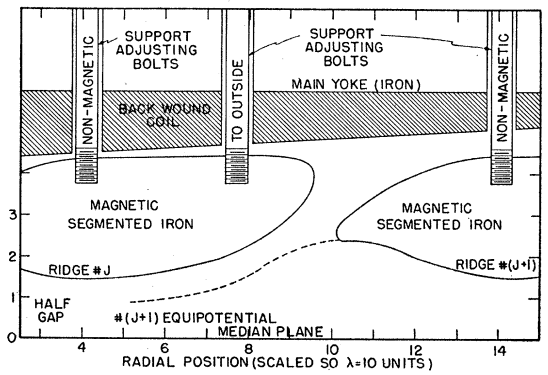

FIG. 18. Floating equipotentials which produce sinusoidal field variation.

The most promising method of decreasing ζ and hence decreasing the nonlinearities so that the stability limit is increased is to use magnets which produce a large flutter, f. Two very promising cases of this type follow:

One case has rectangular ridges of iron with the gap between ridges $\frac{1}{4}$ as big as the gap at the valleys. (See Fig. 19.) Taking account of the fringing flux, we can produce an $f=\sqrt{2}\langle\Delta H\rangle_{\rm rms}/\bar{H}=0.71$ in the favorable case of $A=2$ and $D=9$, where A and D are in units of half-gaps. If we want $f/w=330$, as in the previous example, then $w=0.00215$. This case gives a good size for the injection aperture:

$$G=[4\pi w/(A+D)]\times 4688 \text{ cm}=11.1 \text{ cm}.$$

The circumference factor is less than $(A+D)/(A+\frac{1}{4}D)=2.3$ which could be tolerated at the injection radius. If we do not require that the equilibrium orbits scale, then the ridge proportions can change and the circumference factor can be improved at the high-energy radius. For example, a gradual transition could be made to $A=9$, $D=8$, and $G=7$ cm, with the same f/w including fringing effects. The circumference factor, including fringing effects, is then 1.38.

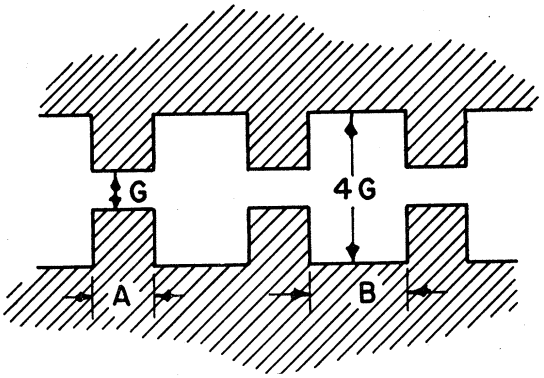

FIG. 19. Rectangular spiral ridges. The distributed back-winding is circumferential.

A structure which has many desirable features is a separated spiral-sector magnet. By winding each spiral ridge separately with a forward coil and with distributed back-windings on the pole face (in the manner shown in Fig. 12 for radial sector magnets), the ridges can be spaced widely enough to bring the field down to approximately zero between ridges; this increases f greatly. If the field shape is that shown in Fig. 20, which gives a circumference factor of 2, the flutter f is 1.28 and the gap can be about 30 cm. The angle between the sector edge and the orbit is large enough to allow a large-amplitude betatron oscillation before the stability limit is reached—possibly as much as 90-cm amplitude. Sector dimensions are shown in Fig. 21.

The gap at the high-field radius can be made much less than 30 cm in order to conserve power, but it is highly desirable to keep this large gap at the low-energy radius for injection purposes.

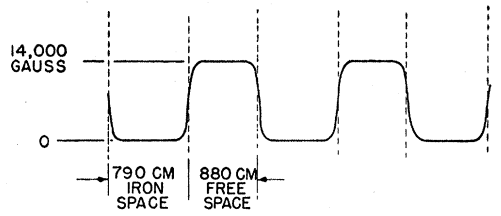

FIG. 20. Circumferential distribution of axial field for separated spiral sectors, at 10 000-cm radius with 30-cm gap.

While this structure requires a large circumference (not all occupied by iron), it has many conveniences compared to magnets already described. The fabrication has simplifying features. The vacuum tube is more easily constructed. Access to the beam for targets is better. The sectors can be separated more where longer straight sections are desired and scaling is still possible. The nonlinear stability limit should be comfortably large, permitting a large useful injection aperture.

14. FFAG Betatrons

The large momentum spread which can be held by FFAG magnets allows a great increase in the acceptance time of injected particles if betatron acceleration is used.[4] The injected particles may be accepted into stable orbits in the dc magnet gap at the low-energy radius all the time that the central magnetic flux is rising; as the particles gain energy, they spiral toward the high-field radius. After each particle orbit has linked a certain change of flux, $\Delta\phi$, corresponding to an increase in momentum to its final value, it reaches the target (or ejector) radius. Charged particles continue to arrive at the target as long as the flux continues to rise beyond $\Delta\phi$. If $\Delta\phi$ is less than the maximum core flux, ϕ_0, useful injection and ejection may occur as much as 25% of the time by cycling the core flux between $+\phi_0$ and $-\phi_0$. When sinusoidal core excitation is used, the duty factor D (the fraction of time for useful

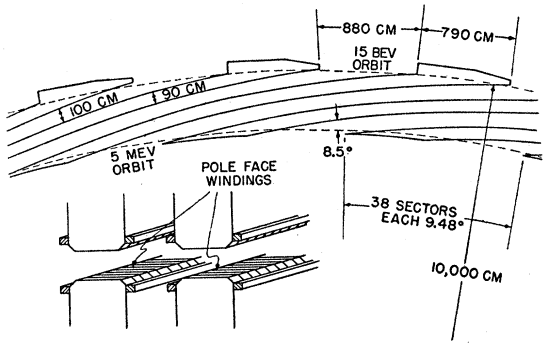

FIG. 21. Separated spiral-sector geometry. Each ridge has its own windings.

injection) is given as follows (see Fig. 22):

$$D=\frac{1}{2\pi}\cos^{-1}\left[\frac{\Delta\phi}{\phi_0}-1\right]. \tag{14.1}$$

In order to miss an injector structure, a certain minimum rate of acceleration (rate of rise of flux) at injection is required; this will reduce the duty factor in practice.

Since the particle equilibrium orbit is not circular and since its radius changes with acceleration, the relationship between $\Delta\phi$ and the momentum increase differs from that for conventional betatrons.

The voltage gain per revolution is, in Gaussian units,

$$V=(1/c)(d\phi/dt), \tag{14.2}$$

where ϕ is the flux in the betatron core. The rate of increase in energy is therefore

$$\frac{dE}{dt}=\left(\frac{e\omega}{2\pi c}\right)\frac{d\phi}{dt}, \tag{14.3}$$

where $\omega/2\pi$ is the frequency of revolution [Eq. (10.3)]. We have, therefore,

$$Rdp=\frac{dE}{\omega}=\left(\frac{e}{2\pi c}\right)d\phi, \tag{14.4}$$

and the required accelerating flux change is determined by

$$\phi_2-\phi_1=\frac{2\pi c\bar{R}}{e}(p_2-p_1), \tag{14.5}$$

where

$$\bar{R}=\frac{1}{p_2-p_1}\int_{p_1}^{p_2}Rdp. \tag{14.6}$$

If k is constant, we have, by Eq. (5.14),

$$\bar{R}=R_2\left(\frac{k+1}{k+2}\right)\frac{1-(p_1/p_2)^{(k+2)/(k+1)}}{1-(p_1/p_2)}$$

$$\doteq\left(\frac{k+1}{k+2}\right)R_2, \quad \text{if} \quad p_1\ll p_2. \tag{14.7}$$

With FFAG guide fields in the 20- to 300-Mev energy range, the duty factor could be increased by more than a factor of 10^4 over that in existing betatrons and synchrotrons. The beam current increase would probably be less because of space-charge effects at injection.

In pulsed-field betatrons, large amounts of energy are stored in the pulsed-guide field magnet gap, and equipment capable of handling the large circulating currents and voltages must be used. In FFAG betatrons, only the accelerating core is pulsed, and it would be a closed iron circuit which would require much less energy storage, and therefore a much smaller condenser bank and less ac power equipment.

Either the radial-sector or the spiral-sector type of FFAG magnet could be used for electron betatron acceleration up to a few hundred Mev, and the design would be subject to the same considerations as discussed above for synchrotrons. Since the core flux change for a given particle momentum increase is proportional to the particle period of revolution, the smaller circumference of the spiral sector type is doubly important for betatrons. In focusing magnets designed for the betatron energy range, an N of 10 to 30 appears more suitable than the higher N values suggested for multi-Bev synchrotrons.

The output beam of electrons from an FFAG betatron would be nearly monoenergetic and spread over a long time corresponding to the duty factor. Present betatrons and synchrotrons achieve a lengthened output beam pulse at the expense of energy homogeneity, since the electrons are in a sinusoidally varying field at essentially constant radius. This and the prospect of beam currents approaching time-average values of milliamperes makes this an attractive accelerator for electrons from a few Mev to several hundred Mev.

15. FFAG Cyclotrons

To make semirelativistic particles revolve in a cyclotron at constant frequency and in orbits that are approximately circles, it is necessary to have the average magnetic field increase with radius. In order to avoid the resultant axial defocusing, alternating-gradient focusing may be employed. There are a number of possible magnetic field configurations for such a fixed-field alternating-gradient cyclotron. The first such cyclotron was proposed by Thomas.[5] The Thomas cyclotron is essentially a radial-sector FFAG machine having three or more sectors with a roughly sinusoidal field flutter. Thomas showed that such a machine has stable orbits for energies up to a limit depending upon the number of sectors. A considerable amount of experimental and theoretical work on the Thomas

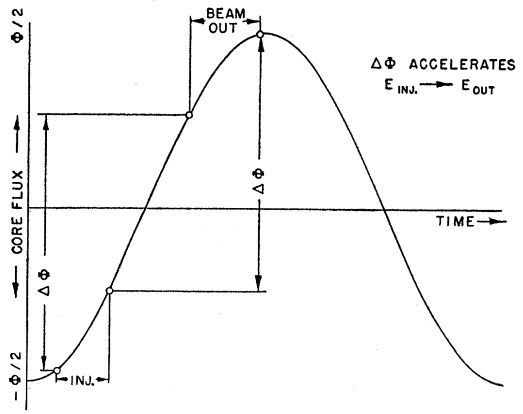

FIG. 22. Time dependence of betatron flux showing duty factor.

cyclotron has been carried out at the University of California, culminating in the successful construction and operation of two electron models which accelerate electrons up to half the speed of light.[18] We will here discuss briefly the general features of FFAG cyclotrons with particular reference to spiral-sector configurations.

In Sec. 10, we have obtained a relation (10.9) between the total energy E and the mean field index k for a cyclotron, in which the frequency of revolution is independent of energy. We have also the approximate expressions developed in Sec. 7 relating k to the betatron oscillation frequencies. For spiral sectors, the simple approximate relation (6.24) holds:

$$\nu_x=(1+k)^{\frac{1}{2}}. \tag{15.1}$$

According to Eq. (10.9), ν_x is given directly in terms of the energy by the relation

$$\nu_x \doteq E/E_0. \tag{15.2}$$

It is clear that the orbits in such a cyclotron start at the center at $E=E_0$ with $\nu_x=1$ (as in a conventional cyclotron), and that as E increases, successive integral and half-integral radial resonances are encountered at energies which are approximately integral and half-integral multiples of E_0. If we regard the first integral resonance as the limiting energy, then the maximum kinetic energy is about one rest energy (actually somewhat less, according to more accurate calculations[19]). If sufficiently high dee voltage is applied, and if magnetic field errors are sufficiently small, it may be possible to drive the particle energy through resonances fast enough to avoid buildup of oscillations. In any case, for stability, ν_x must be less than $\frac{1}{2}N$, so that E can never be greater than about $\frac{1}{2}NE_0$. The predicted existence (Sec. 9) of a strong third integral resonance at $\sigma_x=2\pi/3$, $(\nu_x=N/3)$, may set an even lower limit on E for a given number of sectors N.

In a *radial*-sector configuration in which the number of sectors is small $(N<8)$, the alternating-gradient focusing also comes primarily from the η term in Eq. (5.13), and consequently the relations (15.1) and (15.2) are still roughly correct and the preceding considerations are still qualitatively correct. In particular, this is true of a Thomas cyclotron.

In a cyclotron in which the η term in Eq. (5.13) predominates, we see from Eqs. (6.24) and (6.25) that the focusing depends on k and on the quantity

$$F=2\left\langle\left(\frac{1}{\eta}\frac{\partial\eta}{\partial\Theta}\right)^2\right\rangle_{\text{Av}}+\tfrac{1}{2}f^2. \tag{15.3}$$

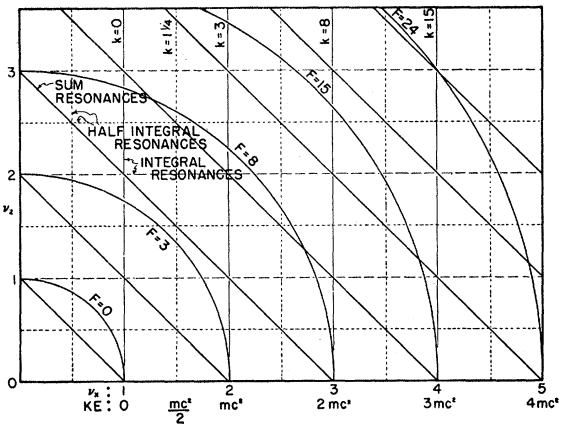

FIG. 23. Working point diagram for a spiral-sector cyclotron. F is the AG focusing parameter.

The focusing parameter F is determined, according to Eqs. (6.24) and (6.25), by the relation

$$F=\nu_x^2+\nu_z^2-1. \tag{15.4}$$

In Sec. 6, we have noted that with spiral sectors, the optimum flutter factor f is about $\frac{1}{4}$, for maximum vertical aperture without extra forward pole-face windings. With this value of f, the focusing parameter F may be written, with the help of Eq. (6.26),

$$F\doteq\tfrac{1}{16}(\tan^2\zeta+\tfrac{1}{2}). \tag{15.5}$$

In Fig. 23, we plot circles of constant F *vs* ν_x and ν_z. Vertical lines of constant k (hence constant E) are marked in the figure. We show also lines representing integral and half integral resonances (ν_x, ν_z=integer or half-integer) and sum resonances ($\nu_x+\nu_z$=integer). As the energy increases from E_0 to E, the working point (ν_x,ν_z) will trace out a curve connecting the line $k=0$ with the line $K=(E/E_0)^{\frac{1}{2}}-1$. The form of this working point curve will depend on the way F varies with radius. In a practical magnet, F will almost necessarily be zero at the center so that the curve will start near $(\nu_x=1, \nu_z=0)$. Difficulties may be expected in accelerating particles beyond a point where the working point crosses any of the resonance lines, particularly integral resonances, or resonances involving the vertical motion (since the vertical aperture is not large). It is clear from Fig. 23 that the working point necessarily crosses a half-integral radial resonance near $E=E_0+\frac{1}{2}E_0$, and a sum resonance and an integral radial resonance before reaching $E=2E_0$.

In order to get a picture of an FFAG cyclotron, we note that the frequency of revolution of an ion in a cyclotron is

$$\omega/2\pi=\beta c/2\pi R=c/2\pi\lambda\!\!\!^{-}, \tag{15.6}$$

where $2\pi\lambda\!\!\!^{-}$ is the wavelength of the radio-frequency voltage required to drive the dees (we assume first-harmonic operation). We have therefore the following

[18] D. L. Judd, Phys. Rev. **100**, 1804(A) (1955); Pyle, Kelly, Richardson, and Thornton, Phys. Rev. **100**, 1804(A) (1955); Heusinkveld, Jakobson, Ruby, Smith, and Wright, Phys. Rev. **100**, 1804(A) (1955). We are indebted to Dr. Judd for a discussion of the work done at Berkeley, which is described in University of California Radiation Laboratory Reports No. 2344 and No. 2435 (unpublished).

[19] D. S. Falk and T. A. Welton, Bull. Am. Phys. Soc. Ser. II, 1, 60 (1956).

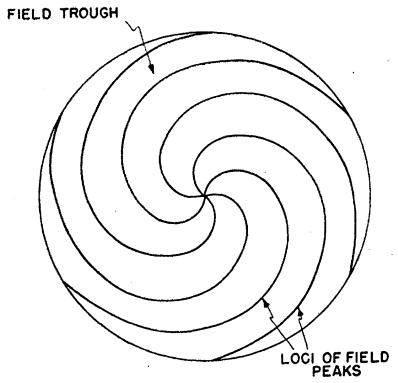

FIG. 24. Plan view of ridges in a 6-sector spiral-sector cyclotron.

relation between energy and radius:

$$E/E_0=\lambda\!\!\!^{-}/(\lambda\!\!\!^{-2}-R^2)^{\frac{1}{2}}. \tag{15.7}$$

The momentum $p(R)$ is

$$p=mcR/(\lambda\!\!\!^{-2}-R^2)^{\frac{1}{2}}, \tag{15.8}$$

the mean magnetic field is

$$\bar{H}=\frac{pc}{eR}=\frac{mc^2/e}{(\lambda\!\!\!^{-2}-R^2)^{\frac{1}{2}}}, \tag{15.9}$$

and the mean field index [Eq. (10.9)] is

$$k=R^2/(\lambda\!\!\!^{-2}-R^2). \tag{15.10}$$

The relations (15.6)–(15.10) are exact. In order to determine the shape of the spiral ridges, we must solve the equations for betatron oscillations. We can get a rough idea of the ridge pattern from the approximate relations (15.1), (15.4), and (15.5). If we combine these formulas with (15.10), we obtain

$$\tan^2\zeta=\frac{16R^2}{\lambda\!\!\!^{-2}-R^2}+\nu_z^2-\tfrac{1}{2}. \tag{15.11}$$

Let us now assume for example that the working point

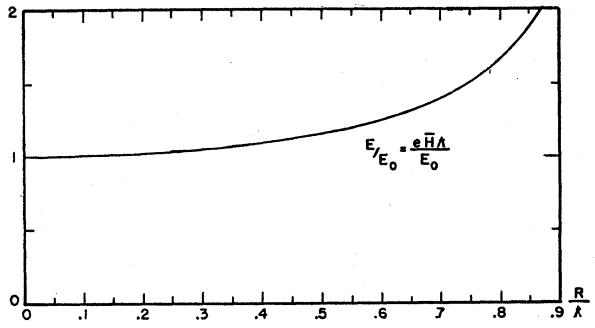

FIG. 25. Total energy and magnetic field as a function of radius in a constant-frequency cyclotron. (E_0 is the rest mass and $2\pi\lambda\!\!\!^{-}$ is the oscillator wavelength.)

in Fig. 23 moves along the horizontal $\nu_z=1/\sqrt{2}$, so that

$$\tan\zeta\doteq\frac{4R}{(\lambda\!\!\!^{-2}-R^2)^{\frac{1}{2}}}. \tag{15.12}$$

If we neglect the scalloping of the equilibrium orbit, we may replace R by the radius r, and substitute in Eq. (6.30) to obtain the equation for a spiral ridge in polar coordinates:

$$\theta_0=4\sin^{-1}(r/\lambda\!\!\!^{-}). \tag{15.13}$$

If we assume a sinusoidal field flutter, the function μ is

$$\mu=1+\tfrac{1}{4}\cos[N(\theta-\theta_0)], \tag{15.14}$$

and the magnetic field is given by

$$H=\bar{H}\mu=\frac{mc^2/e}{(\lambda\!\!\!^{-2}-R^2)^{\frac{1}{2}}}\times\{1+\tfrac{1}{4}\cos[N\theta-4N\sin^{-1}(r/\lambda\!\!\!^{-})]\}. \tag{15.15}$$

The number of sectors N is, to this approximation, still arbitrary. If the output energy is to be $E=2E_0$, (about 1-Bev kinetic energy for protons), then $\nu_x\doteq 2$ at the output radius, and N must be at least 4, for linear stability of the betatron oscillations. In order to avoid the third integral nonlinear resonance at $\sigma_x=2\pi/3$, we should probably take $N=6$. In Fig. 24, we plot the ridges and troughs given by Eq. (15.13) for a cyclotron with six spiral sectors and an output energy $E=2E_0$. In Fig. 25, we plot E and $\bar{H}$ *vs* R for such a cyclotron.

ACKNOWLEDGMENTS

We wish to acknowledge many helpful discussions with H. R. Crane, F. T. Cole, Nils Vogt-Nilsen, J. N. Snyder, and other members of the Midwestern Universities Research Association technical group.

APPENDIX A. THE SMOOTH APPROXIMATION

Let the alternating-gradient equation of motion in one dimension be written in the form

$$d^2x/d\theta^2=f(x,\theta), \tag{A.1}$$

where the force $f(x,\theta)$ is periodic in θ with period $2\pi/N$. We will assume that $N\gg\nu$, that is, that the betatron wavelength is long compared with the sector length. It is then reasonable to seek an approximate solution of the form

$$x=X+\xi(X,\theta), \tag{A.2}$$

where the "smooth" oscillation $X(\theta)$ satisfies an equation of the form

$$d^2X/d\theta^2=F(X), \tag{A.3}$$

independent of the sector periodicity, and the "ripple" $\xi(X,\theta)$ is periodic in θ with period $2\pi/N$ and with zero mean, for fixed X. We will assume that the ripple ξ

and the derivatives $dX/d\theta$, $d^2X/d\theta^2$ are small in a sense to be made more precise presently.

We substitute Eq. (A.2) in (A.1) to obtain

$$X''+\xi_{\theta\theta}+2\xi_{X\theta}X'+\xi_{XX}X'^2+\xi_X X''=f(X+\xi,\theta), \quad \text{(A.4)}$$

where primes deonote derivatives with respect to θ. We now average over θ, keeping X, X', X'' fixed, remembering that $\langle\xi\rangle_{Av}=0$, to obtain an equation corresponding to (A.3):

$$d^2X/d\theta^2=\langle f(X+\xi,\theta)\rangle_{Av}. \quad \text{(A.5)}$$

We subtract Eq. (A.5) from (A.4):

$$\xi_{\theta\theta}=\{f(X+\xi,\theta)\}-2\xi_{X\theta}X'-\xi_{XX}X'^2-\xi_X X''. \quad \text{(A.6)}$$

We use the notation introduced in the definition (4.14). It is easy to see that the last two terms are of order $(\sigma/2\pi)^2$ relative to the first term, and are therefore negligible if $N\gg\nu$. The second term is only of order σ/π relative to the first, but its effect on the smooth equation (A.5) can be shown to cancel out to first order. We therefore neglect the last three terms in Eq. (A.6) and replace $\{f(X+\xi,\theta)\}$ by $\{f(X,\theta)\}$, i.e., we assume that $\{\xi f_X\}\ll\{f\}$. We can then integrate Eq. (A.6) to obtain, as a first approximation to the ripple,

$$\xi=f_2(X,\theta), \quad \text{(A.7)}$$

in the notation introduced in definitions (4.16) and (4.17). If we substitute the ripple (A.7) in Eq. (A.5), we obtain, to first order in ξ, the smooth approximation

$$d^2X/d\theta^2=\langle f\rangle_{Av}+\langle f_2 f_X\rangle_{Av}. \quad \text{(A.8)}$$

(Essentially the same result has been obtained by Sigurgiersson.[20]) To the solution of Eq. (A.8) is to be added the ripple (A.7) to obtain an approximate solution to Eq. (A.1). The second term on the right in Eq. (A.8) can be integrated by parts and rewritten in the form

$$d^2X/d\theta^2=\langle f\rangle_{Av}-\langle f_1 f_{X1}\rangle_{Av}. \quad \text{(A.9)}$$

If the force in Eq. (A.1) is linear in x,

$$f(x,\theta)=g(\theta)x, \quad \text{(A.10)}$$

then Eq. (A.9) can be written as a linear equation

$$d^2X/d\theta^2=[\langle g\rangle_{Av}-\langle g_1^2\rangle_{Av}]X, \quad \text{(A.11)}$$

and the approximate solution (A.2) then can be written in the Floquet form

$$x=e^{\pm i\nu\theta}[1+g_2(\theta)], \quad \text{(A.12)}$$

where

$$\nu^2=\langle g_1^2\rangle_{Av}-\langle g\rangle_{Av}. \quad \text{(A.13)}$$

The above results can be immediately generalized to the two-dimensional case

$$\begin{aligned} d^2x/d\theta^2&=f(x,z,\theta),\\ d^2z/d\theta^2&=g(x,z,\theta). \end{aligned} \quad \text{(A.14)}$$

We assume a solution of the form

$$\begin{aligned} x&=X+\xi,\\ z&=Z+\zeta. \end{aligned} \quad \text{(A.15)}$$

We have the approximate equations

$$\begin{aligned} \xi&=f_2(X,Z,\theta),\\ \zeta&=g_2(X,Z,\theta), \end{aligned} \quad \text{(A.16)}$$

where X, Z satisfy

$$\begin{aligned} d^2X/d\theta^2&=\langle f\rangle_{Av}+\langle f_2 f_X\rangle_{Av}+\langle g_2 f_Z\rangle_{Av},\\ d^2Z/d\theta^2&=\langle g\rangle_{Av}+\langle f_2 g_X\rangle_{Av}+\langle g_2 g_Z\rangle_{Av}, \end{aligned} \quad \text{(A.17)}$$

where averages are over θ with X, Z fixed.

In practice, we have found that Eq. (A.13) gives values of ν or $\sigma(=2\pi\nu/N)$ which are accurate to within about 10% of $[\langle g_1^2\rangle_{Av}]^{\frac{1}{2}}$, provided that $[\langle g_1^2\rangle_{Av}]^{\frac{1}{2}}\lesssim N/4$. A few nonlinear cases have been studied, and solutions of Eqs. (A.8) and (A.17) have yielded results in fair agreement with more accurate calculations except near stability boundaries. Stability boundaries where the betatron wavelength becomes infinite are fairly accurately predicted by Eqs. (A.8) and (A.17) but the (more interesting) stability boundaries due to sector resonances when the betatron wavelength becomes a small integral number of sectors are not predicted at all by the smooth equations.

[20] T. Sigurgiersson, CERN report, CERN-T/TS-1, December, 952; CERN-T/TS-3, May, 1953 (unpublished).